NTNU

Norwegian University of
Science and Technology

REGENERATION IN CRANE OPERATIONS

Jan Olav Øksnes

Master of Science in Engineering and ICT
Submission date: August 2017
Supervisor: Eilif Pedersen, IMT
Co-supervisor: Stian Skjong, IMT

Norwegian University of Science and Technology
Department of Marine Technology

MASTER THESIS IN MARINE ENGINEERING

SPRING 2017

FOR

STUD. TECHN. JAN OLAV ØKSNES

REGENERATION IN CRANE OPERATIONS

Work Description: Crane operations on board cargo ships have traditionally used hydraulic actuators. The potential energy released when lowering the cargo is simply burned on brakes. If instead there were a system to regenerate the energy, the potential savings in both local pollution and fuel savings could be significant. One way to store the regenerated energy is to use electrical actuators and battery packs. Once the ship has a battery pack, it is also possible to implement hybrid control schemes, like peak shaving. If the battery pack is big enough to count as a spinning reserve, one might also reduce the number of generator sets and still satisfy the redundancy requirements.

The main objective of this master thesis is to execute a case study which aims to unravel the advantages of implementing a regenerative control scheme using a battery pack in electric crane operations on board a cargo ship. The study will use a crane model that is based on the model that was created in the master thesis by Fredrik Gyberg 2017. The first objective is to review the model and implement the functionality needed to connect the crane to the electrical grid. The generator set and battery pack models, supplied by the institute, will be implemented to power the crane and store the regenerated power. The measurement data supplied by Grieg Star will then be used to calibrate the final model, to ensure that the crane model behaves like the real crane.

If time permits, there will be created a proposition on how the regenerative functionality can be implemented on the physical crane model made by Fredrik Gyberg 2017.

Scope of work

1. Review the crane model created in the master thesis by Fredrik Gyberg 2017 and implement the following features:
   (a) Implement a cable model with winch adding hoisting functionality, so the model can lift and lower the hoisting cable.
   (b) Implement electric actuators in the slewing, luffing and hoisting motion, focus on the winch model so the crane can exchange power with the electric grid.
2. Complete the simulation model by implementing a generator set and battery bank model.
3. Calibrate and verify the model by running simulations on the same load cycles that were used in the measurement data supplied by Grieg Star.
4. Set up a case study that measures the fuel consumption of four cranes executing the same load cycle with random time intervals, with and without the regenerative system.
5. *If time permits*: Design the implementation of the regenerative system onto to the physical lab crane created by Fredrik Gyberg.

The report shall be written in English and edited as a research report including literature survey, description of mathematical models, description of control algorithms, simulations results, discussion and conclusion including a proposal for further work. Source code developed shall be provided on a CD or equivalent with code listing enclosed in appendix.

The Department of Marine Technology, NTNU, can use the results freely in its research work by referring to the students work.

The thesis should be submitted in three copies within 23th August 2017.

Trondheim March, 2017
Supervisor: Associate Professor Eilif Pedersen
Co-Supervisor: PhD Candidate Stian Skjong

Preface

This master's thesis is submitted to the Norwegian University of Science and Technology (NTNU) in fulfilment of the requirements for the degree Master of Science in Marine Technology.

The start date was delayed for 2 months due to a combination of voluntary work and a course I had to take in the spring semester, to get enough study points to complete the master's degree. Even though the start date was delayed, there was little progress before the last exam was finished in the beginning of June. So this summer has been tough. Thus it is with the utmost joy that I now can look back at the whole process, and say that I am finished!

I would like to thank Roar Fanebust at Grieg Star and Tomas Tengner at ABB AS Marine and Ports for taking their time to answer my questions regarding Grieg Star's power systems and ABB's energy storage solutions. Their information has been vital in the modelling process.

I would like to extend a special thank my supervisor Associate Professor Eilif Pedersen and my Co-Supervisor PhD Candidate Stian Skjong for allot of good advice and guidance during the project.

Trondheim, August 23^{th}, 2017
Jan Olav Øksnes

Abstract

In this thesis a marine power plant with a battery pack has been modelled using bond graph theory, using the bond graph simulation software 20-sim. The popularity of hybrid power systems is increasing in the marine sector, mainly because it is an effective way to reduce fuel consumption, emissions and maintenance costs. Three control strategies were created to test the model, where each strategy had a different focus. A new control strategy was developed after case study one, where each of the control strategies were tested. The new control strategy, which then would be used in case study two, combined two of the previously tested strategies, to gain the benefits of both.

In case study 2, which was this thesis main case study, the results of two simulations where compared. One simulation ran two gensets, and the other ran one genset assisted by a battery pack. The load profile applied was set to resemble an electric crane operation on a dry bulk carrier. The results show that if one genset is replaced with a 362 kWh battery pack, the fuel consumption rate can be reduced by 9.23%, while the maintenance costs for the operation can be reduced by over 50%. The figures are believed to be conservative, since the battery pack model's efficiency rating is lower than the real battery pack, due to an added resistance to make the model stable. The results show that implementing a battery pack can give significant reductions both environmentally and economically, and should be implemented on all ships that have a diesel-electric power system.

Contents

List of Figures

List of Tables

1 Introduction

1.1 Background and Motivation

One of the greatest threats of the 21st century is the increasing pace of global warming. Fossil fuel emissions are attributed as one of the leading causes of global warming (Zecca and Chiari (2010)); thus the most efficient way to fight global warming is to reduce our consumption of fossil fuels. Simultaneously as we need to reduce our dependency on fossil fuels, the world's energy demand is calculated to double, from 14 TW in 2015 to 28 TW in 2050 (Tarascon (2015)). Even though the use of wind, solar thermal, solar PV and geothermal energy are expanding rapidly (+16.8%, +6.8%, +29.7%, +4.1% respectively in 2014), it still contributes less than 2% of the world's total energy, in comparison to fossil fuels, which accounted for 81.7% of the world's energy production in 2014 (International Energy Agency (IEA) (2017)).

Shipping is the most energy efficient way to transport large quanta of goods. To put things in perspective, in 2015, world seaborne trade volumes are estimated to have accounted for over 80% of total world merchandise trade (United Nations Conference on Trade and Development (2017)). Since shipping is such an integral part of the world's trade, they also stand for a big chunk of the world's annual greenhouse gas emissions. For the period 2007–2012, on average, shipping accounted for approximately 3.1% of annual global CO_2 and approximately 2.8% of annual greenhouse gasses (International Maritime Organization (IMO) (2014)). The Maritime CO2 emissions are projected to increase significantly in the coming decades.The increase is projected to be between 50% to 250% in the period to 2050, depending on future economic and energy developments according to (International Maritime Organization (IMO) (2014)). With this development in mind, it is clear that the shipping industry has to contribute a lot if we are going to meet the internationally agreed goal of keeping global temperature increase to below 2°C compared to pre-industrial levels, which requires worldwide emissions to be at least halved from 1990 levels by 2050.

The IMO has created a set of regulations to ensure that the shipping industry invests in pollution reducing measures. E.g. the regulations for nitrogen oxides (NO_x)(Regulation 13) and sulphur oxides (SO_x)(Regulation 14). The NO_x regulations apply to engines installed on a ship, with a power output of more than 130 kW, and sets the limit for NO_x emissions based on the engine's age and rated speed, where the limit is stricter for newer engines. The SO_x regulations limits the sulphur content of any fuel oil used on board ships. They have provided three limits where the loosest one was before 2012, and the strictest is for after 2020. Both regulations are found in "Annex VI: Regulations for the prevention of air pollution from ships" of MARPOL (International Maritime Organization (IMO) (2011)). IMO has introduced an energy efficiency design index (EEDI) that is mandatory for all new trade ships after 2013. The EEDI measures a ship design's emission rate in grams of CO_2 per tonne mile, where a lower EEDI is less polluting and aims at promoting the use of more energy efficient equipment and engines. The EEDI requirement was set to a 10% reduction from the base line set in 2013 and is set to be tightened every five years to keep pace with technological developments.

The author's main motivation for writing this thesis is to highlight both the economical and emission reducing advantages of implementing battery packs on board ships. It is important that the economical benefits of this are conveyed to the shipping industry, such that the industry embraces it, and thus contributes to a reduction of both global and local emission problems.

The scope of work has been altered from the original, that can be seen at the beginning of this thesis. The original scope of work states that the power system model should be implemented in a crane model, which was created by Fredrik Gyberg in his master's thesis. That plan was found to be too complex, both with regards to modelling and computational power, i.e. simulation

speed. Thus the crane model was not included, and the load was applied directly based on test data from Grieg Star.

1.2 Related Work

The two main references used for bond graph theory are Borutzky (2009) and Pedersen and Engja (2014). They present the fundamental concepts, modelling approaches, techniques and software tools that support the process of bond graph based physical systems modelling.

Scrosati and Garche (2010) gives a thorough discussion on the current status of lithium ion batteries, their near-term improvements in specific energy, power and safety and reliability. In the end, they investigate some of the most promising long-term developments. Weicker (2013) starts with the lithium-ion battery fundamentals and goes on with a review of battery management architectures, measurements, control and functionality.

There are two major approaches to modelling batteries: electrochemical models and equivalent-circuit models. Martínez-Rosas et al. (2011) and Ménard et al. (2010) presents electrochemical models while Hu et al. (2012) and He et al. (2012) are comparative studies of equivalent-circuit models. Erdinc et al. (2009) has created an augmented equivalent-circuit model that can predict the effects of temperature and capacity fading on the battery. Aarflot (2010) investigates the level of battery monitoring that is needed to maintain a sustainable and safe operation of the battery.

As for similar studies, Ovrum and Bergh (2015) concluded that cargo ships with electrical cranes could save $110,000 per year from crane operations on the ship alone, where the annual savings of the hybrid solution amount to a third of the battery costs.

Geertsma et al. (2017) is a review of the developments in design and control of hybrid power and propulsion systems for smart ships. They conclude that hybrid architectures with advanced control strategies can reduce fuel consumption and emissions up to 10–35% while improving noise, maintainability, manoeuvrability and comfort.

1.3 Structure of the Thesis

This section presents the structure of this thesis.

Chapter 2: Provides the reader with some background theory for the different topics that are used in the modelling later on.

Chapter 3: Modelling of the power plant and battery. Presents all the equations needed to construct the model.

Chapter 4: Discusses different control strategies that will be tested later on.

Chapter 5: Contains the case studies. Each case study's setup is described in detail before the results are presented and discussed.

Chapter 6: Conclusion and proposed further work. The main results in the thesis are summarised and discussed, and suggestions for further studies and work are given.

Appendix A: List of attachments

Appendix B: Tables of parameters used in this thesis.

2 Background Material

2.1 Diesel-electric Propulsion

Diesel-electric propulsion became popular during the 80's and 90's when the possibility to control electrical motors with variable speed in a large power range with compact, reliable and cost-competitive solutions were introduced. Today diesel-electric propulsion is widely used in ships that operate with large variations in load demand, e.g. Ferries and DP drilling vessels. It is also popular in, e.g. cruise ships, where the noise reduction is important for the customer's comfort (Ådnanes (2003)).

Advantages of diesel-electric power system (Ådnanes (2003)):

- Economic: Reduced fuel consumption and maintenance, especially where there is a large variation in load demand.
- Performance: Better utilisation of on-board space increases the ship's payload. Increased manoeuvrability, since thruster placement can be optimised when the motors are close to the propellers and fed by electric cables.
- Safety: Reduces vulnerability to single point failures, by having several gensets running at separate MSBs, physically separated in different engine rooms.
- Environment: Reduces emissions by only running the necessary genset, compared to constantly running a few large prime movers.
- Comfort: Less vibrations since the propeller shaft is very short.

Disadvantages of diesel-electric power system (Ådnanes (2003)):

- Economic: Increased investment costs. The extra equipment requires
- Performance: Increased transmission losses at full load, caused by the additional components between prime mover and propeller. The efficiency of a diesel-electric system, from diesel engine shaft, to electric propulsion motor shaft, is normally between 0.88 and 0.92 at full load.

The traditional diesel-electric system has AC on the main bus, but in the last 10-15 years, some have started to look at the possibility to have DC on the main bus, e.g. ABB's "Onboard DC Grid" (Lindtjørn and Kanerva (2016)). Currently the solutions are available up the medium voltage level of 1000 V. The main advantages of having DC on the main bus are that the gensets are not forced to work at a set rpm, but can rather run at the most optimal rpm based on the current load level and that it becomes easier to install renewable sources, e.g. batteries. The first installation of ABB's "Onboard DC Grid" was on the platform supply vessel Dina Star in 2013. The owner confirmed significant fuel economic savings, with savings in low load conditions reported of up to 27 percent and 14 percent during dynamic positioning in challenging weather conditions.

2.2 Batteries

Ever since the French physicist Gaston Planté invented the lead-acid battery in 1859, secondary batteries have become a core technology for supporting the development of a sustainable and mobile society. Figure 2.1 shows how the energy density of secondary batteries have increased with 650% since the beginning of the 1950s.

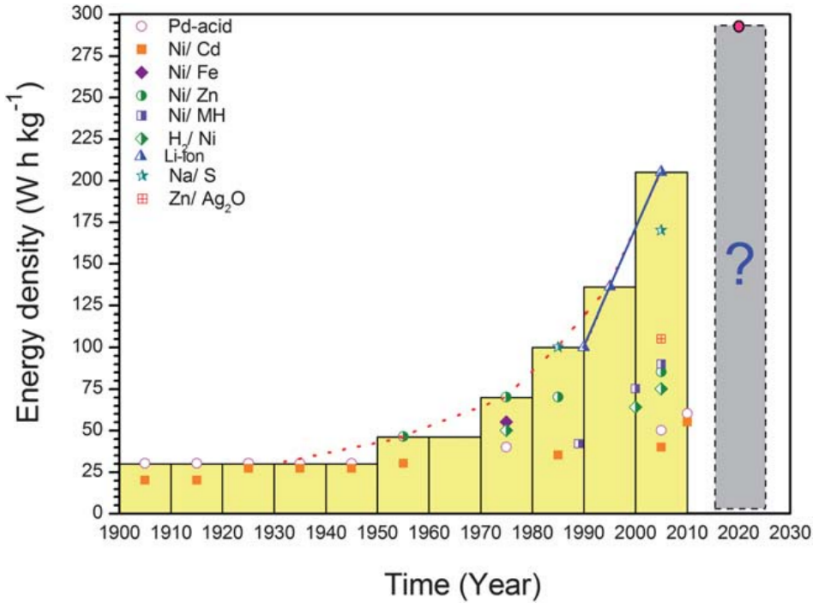

Figure 2.1: Development of energy density in batteries (Zu et al. (2011))

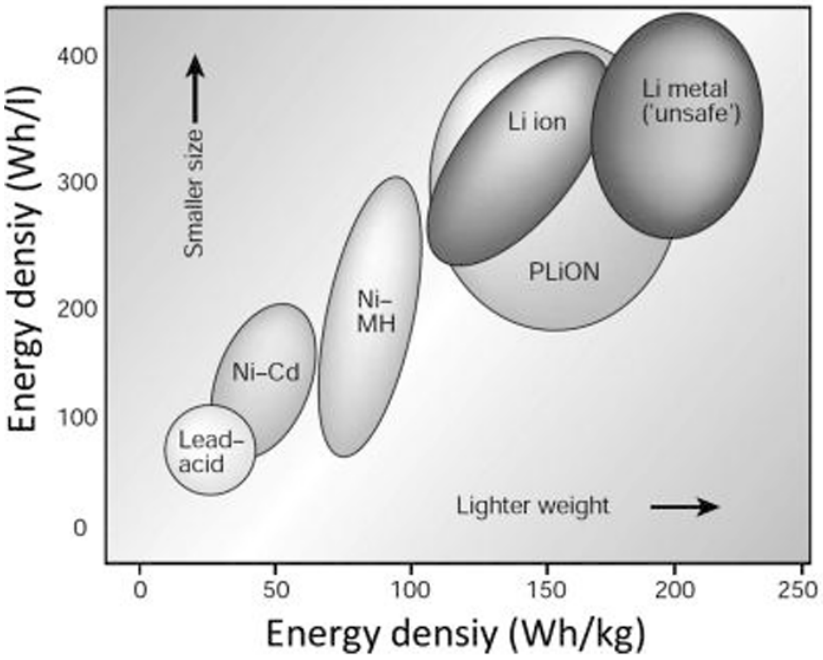

Figure 2.2: Energy density in batteries, weight vs volume (Tarascon (2015))

Both figure 2.1 and figure 2.2 shows that it is the lithium-ion batteries that drive the energy density frontier today, both by mass and volume. It is the development of lithium-ion batteries that have made the portable electric device era that we live in now possible. Initially, the cost of lithium-ion batteries was over \$3,000/kWh. As the use of portable electric devices grew, the prices for lithium-ion fell with an annual rate of more than 10%, leading to a price of under \$300/kWh today(Iizuka et al. (2015)).

The increase in energy density and fall in price made lithium-ion batteries a viable alternative for electric cars, and thus boosted the development of electric cars. The sophisticated hybrid electric and pure electric systems that have been developed for cars are now being adapted by

other transport sectors, e.g. shipping.

There exists a lot of different lithium-ion batteries. They are named after their active cathode materials, where the long chemistry terms often are shortened by abbreviations. One them is the NMC, which has been used successfully in hybrid and electric vehicles due to its high energy and power density, respectable cycle and calendar life, better safety than pure cobalt cathodes, and good performance at extreme temperatures. NMC cathode material is a combination of nickel, manganese, and cobalt oxides (Weicker (2013)). This is the type of battery chemistry that the model will be based on.

2.2.1 Battery Management System

The battery management system primary responsibility is to monitor and prevent the following lithium-ion battery abuse conditions (Weicker (2013)):

Overcharge: Overcharge occurs when a cell is charged to a state of charge greater than 100%. Overcharge causes a number of irreversible degradation mechanisms inside the cell which can lead to an energetic failure. Overcharge can lead to thermal runaway, cell swelling, venting, and other serious events.

Overdischarge: Overdischarge is the discharge of a cell below 0% SOC. Over-discharge can lead to significant internal cell damage including dissolution of the anode foil. Subsequent attempts to recharge a cell that has been deeply and repeatedly overdischarged can lead to safety risks.

High temperature: Exposure to high temperature, in addition to increasing the rate of cell degradation, can lead to thermal runaway, in which the activation temperature of various exothermic chemical reactions inside the cells is reached, and the cell degrades rapidly with a large release of energy, leading to venting of cell contents, temperature increase, fire, or explosion.

Low temperature: Most lithium-ion cells have limited performance, especially charging capabilities at low temperatures. Charging at low temperatures can cause plating of metallic lithium on the anode leading to irreversible capacity loss and the possibility of metallic "dendrite" growth, which can penetrate the separator, causing an internal short circuit. Discharge capability is also limited under low temperature due to increased cell impedance.

Overcurrent: Excessive charge and discharge currents can cause localized overcharge and discharge to occur, leading to the same types of reactions as generalized overcharge and overdischarge. High currents also lead to internal heating, which can lead to over-temperature conditions.

A battery pack consists of many battery cells, where each cell is unique. Even within the same production line, each battery cell will differ microscopically from the others. Therefore it is very important to measure the voltage of each individual cell, to monitor its state of charge. If one cell fails, it can spread to the nearby cells and in the worst case lead to a thermal runaway.

The battery cell's ability to handle large charge and discharge currents is a function of the duration. According to Corvus, a battery with NMC chemistry of the type that is used in this thesis can withstand bursts of C-rate=$\pm$6 for up to 10 seconds without causing an immediately noticeable reduction in SoH. Each burst will cause some amount of damage, so if the bursts occur too regularly, it will reduce the SoH. It all comes down to a trade off between SoH and performance. Batteries packs are often special tailored for the environment they will work in, according to the customer's needs.

To avoid overcharge and overdischarge, Corvus recommended to keep the SoC between 10% and 90%. They also recommended that the C-rates were kept within ±2 most of the time, to assure that the cooling system could cope with the dissipated heat. The information from Corvus was received in a phone call to their sales desk.

For further information on lithium-ion batteries and battery management, the reader is advised to check out Weicker (2013).

2.2.2 Battery Modelling

There are two major approaches to modelling batteries: electrochemical models and equivalent-circuit models. Electrochemical models are only necessary if effects on the battery's SoH or chemical reaction states are of interest, and will therefore not be necessary for this thesis. The reader can check out Martínez-Rosas et al. (2011) and Ménard et al. (2010) for more information and examples on electrochemical models .

The simplest equivalent-circuit model is an ideal voltage source (figure 2.3), that applies a voltage from, e.g. a look-up table based on the battery's SoC. The ideal voltage-source has no dynamics with regards to current fluctuations, which will be significant in a marine power system. Thus this model is not sufficient.

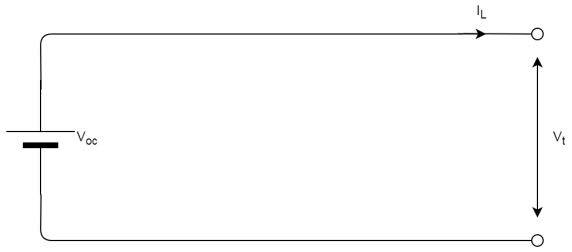

Figure 2.3: Battery model with ideal voltage source

To include the voltage drop that occurs when a current flows through the battery because of the battery's inner resistance, a resistance is added in series with the ideal voltage source (figure 2.4). The ohmic voltage drop is the most significant effect during a simulation that only focuses on power flow. Thus this model would probably be accurate enough. This is also the model that was used in Ovrum and Bergh (2015).

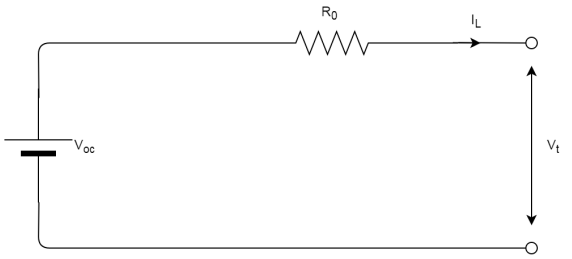

Figure 2.4: Battery model with series resistance

Some of the effects that the series resistance model does not include are (Weicker (2013)):

Polarization or charge transfer resistance: The rate of electrochemical reactions (in this case, the intercalation of lithium ions into the anode and cathode materials) is limited and proceeds at a rate depending on the applied voltage. The Butler-Volmer equation governs this

effect. This effect can be modelled with a resistor known as the charge transfer resistance. The charge transfer resistance increases at low temperature.

Double layer capacitance: The charge transfer resistance causes the accumulation of charge carriers at the surface of the electrode, which creates a capacitor-like effect due to the charge separation across a short distance.

Diffusion: Concentration gradients exist in both electrodes and electrolytes leading to overpotentials.

A model that includes an approximation of these effects is the Thevenin equivalent-circuit model (figure 2.5).

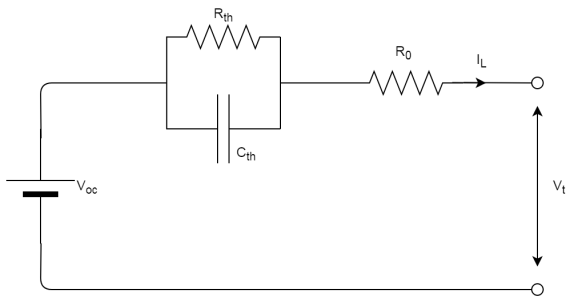

Figure 2.5: Thevenin equivalent battery model

The different dynamics of these three models can be seen in figure 2.6. The first model with only an ideal voltage source (V_{OC}) does not react to the varying current. The second model with the series resistance (V_{Ohmic}) includes the voltage drop caused by the current going through the battery's inner resistance. The Thevenin equivalent (V_{Thevenin}) has a more advanced dynamic response, which captures an approximation of the dynamics listed above. It is unclear if there would have been any significant differences between the results from the series resistance model and the Thevenin equivalent model in this thesis, but the Thevenin equivalent model is chosen as the model to be implemented in the power system.

There exist more advanced equivalent circuits for lithium-ion batteries, but they are not necessary for this thesis. For more information, Hu et al. (2012) and He et al. (2012) are comparative studies of equivalent-circuit models.

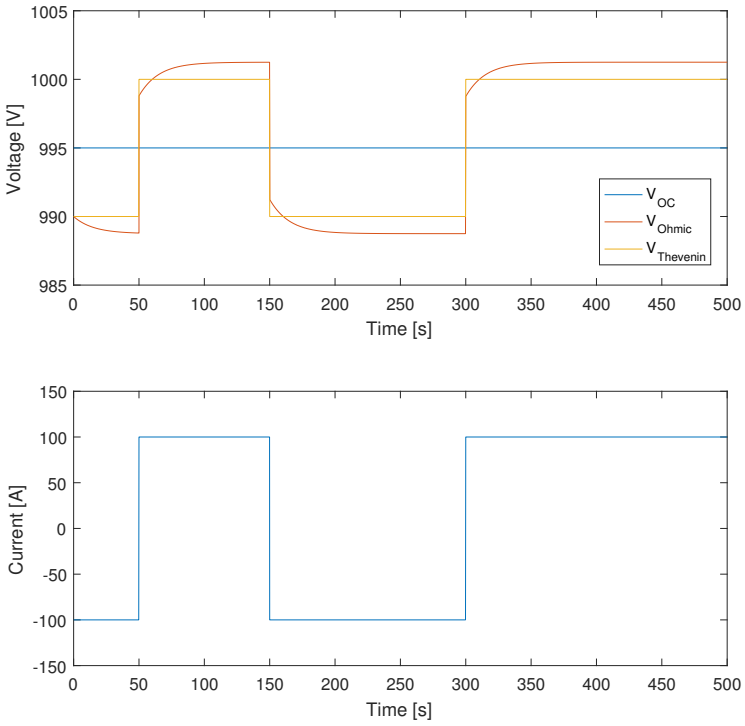

Figure 2.6: Voltage response of the different models

2.3 Power Management System

One of the worst case scenarios on a ship is that a black out occurs. If the ship has no engines on direct propulsion, a black out results in a drifting dead ship until the power system is brought back online, and must be avoided at all costs. To monitor the state of the power system, most ships today use a power management system (PMS). The PMS will start and stop generators if the load level is too high or low for the current load profile.

Some of the benefits of a PMS are listed below (Kongsberg Maritime (2017)):

- Diesel generator monitoring and control
- Diesel engine safety and start/stop
- Circuit breaker synchronize & connect
- Bus line voltage and frequency control
- Generator voltage and frequency control
- Symmetric or asymmetric load sharing
- Load control with load shedding
- Heavy consumers logic
- Automatic start and connect after blackout

Heavy consumer logic: To avoid that heavy consumers, e.g. bow thrusters and ballast water pumps overload the system, the heavy consumer logic makes the consumers send a signal to the PMS before they turn on. The signal tells the PMS how much power the consumer needs and

the PMS then decide if it needs to start up more gensets before the PMS tells the consumer that it is all clear to turn on.

Tripping of non-essential load: If something unforeseen happens and the load level becomes dangerously high, the PMS will trip non-essential loads. The non-essential loads are defined in a prioritised list, where the least important load is cut first. This is an event that should not happen since the PMS should have started another genset before the load level reached the critical limit, but it is the PMS's last defence to avoid a black out. One such unforeseen event could be, e.g. that one of the online gensets fails.

Local PMS: Some systems, like the McGregor cranes used on board Grieg Star's ships, has a local PMS. This means that the ship's PMS has no control and only sends the ships available power to the local PMS. The local PMS uses this information to make sure that the cranes do not overload the system. One of the ways it distributes the power variations over time is by having a 2 s ramp-up time on all hoisting and luffing operations. The cranes are not categorised as heavy load consumers by the ships PMS since they are bounded by the local PMS.

2.4 The Bond Graph

The model will be developed using bond graph modelling. The bond graph provides a graphical modelling approach and is an energy based method to develop mathematical models of physical systems within multiple physical domains. Figure 2.7 presents a list of bond graph variables in different physical domains.

Energy domain	**Effort** (e)	**Flow** (f)	**Momentum** (p)	**Displacement** (q)
Electrical	Voltage $[V]$	Current $[A]$	Flux linkage $[Vs]$	Charge $[As]$ or $[C]$
Mechanical translation	Force $[N]$	Velocity $[m/s]$	Linear momentum $[kgm/s]$	Distance $[m]$
Mechanical rotation	Torque $[Nm]$	Angular velocity $[rad/s]$	Angular momentum $[Nms]$	Angle $[rad]$
Hydraulic	Pressure $[Pa]$	Volume flow rate $[m^3/s]$	Pressure momentum $[N/m^2s]$	Volume $[m^3]$
Thermal	Temperature [K]	Entropy flow $[J/s]$	(not defined)	Entropy $[J]$
Magnetic	Magneto-motive force $[A]$	Flux rate $[Wb/s]$	(not defined)	Flux $[Wb]$
Chemical	Chemical potential $[J/mol]$	Rate of reaction $[mol/s]$	(not defined)	Advancement of reaction $[mol]$

Figure 2.7: Bond graph variables in different physical domains (Pedersen and Engja (2014))

The method is based on the principle that the system dynamics is governed by accumulation,

dissipation and interchange of energy between systems. The power bonds represent pipes that allow energy to flow within a system, thereof the name power bond. The energy flow consists of the variables effort and flow (2.1).

$$\text{Power} = \text{Effort} * \text{Flow} \tag{2.1}$$

The state variables in the mathematical equations that the bond graph generates are the generalised momentum (2.2) and the generalised displacement (2.3).

$$p = \int_0^t e(t)dt + p(0) \tag{2.2}$$

$$q = \int_0^t f(t)dt + q(0) \tag{2.3}$$

A bond graph can represent both nonlinear and linear systems. The basic bond graph consists of nine different elements. These elements are: Effort source (Se), Flow source (Sf), Inertia (I), Capacitor (C), Resistor (R) Transformer (TF), Gyrator (GY), 0-junction and 1-junction. Each element has a constitutive law that governs how it interacts with the surrounding elements. The constitutive relations of the basic bond graph elements can be seen in figure 2.8.

The direction of the power bond acts as a sign convention, defining which way the energy flow is considered to be positive. To be able to derive the state equations of the system, there has to be a way to determine the input-output causality of the graph, i.e. which side of each power bond will set the effort and the flow. To do this, a causality stroke is added to each bond (figure 2.9). The causality stroke states that the side with the stroke will set the flow, while the other side sets the effort. One of the advantages with the bond graph is that it is possible to detect causality problems, e.g. algebraic loops before the equations are written.

The bond graph models are implemented in the bond graph software 20-sim. For a more thorough introduction to bond graph modelling, the reader is advised to check out Borutzky (2009) and Pedersen and Engja (2014).

Bond graph element	Constitutive relations
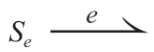	$e = e(t)$
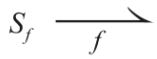	$f = f(t)$
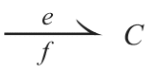	General : $q = \Phi_C(e)$ Linear : $q = Ce$
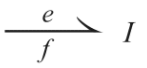	General : $p = \Phi_I(f)$ Linear : $p = If$
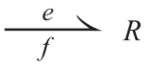	General : $e = \Phi_R(f)$ Linear : $e = Rf$
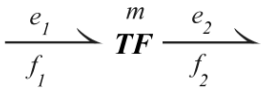	$e_1 = me_2$ $mf_1 = f_2$
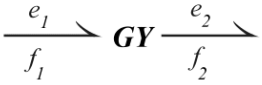	$e_1 = f_2 r$ $f_1 r = e_2$
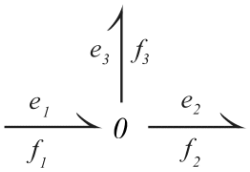	$e_1 = e_2 = e_3$ $f_1 - f_2 - f_3 = 0$
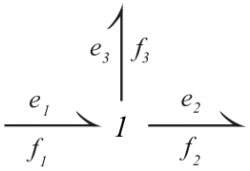	$f_1 = f_2 = f_3$ $e_1 - e_2 - e_3 = 0$

Figure 2.8: Basic bond graph elements (Pedersen and Engja (2014))

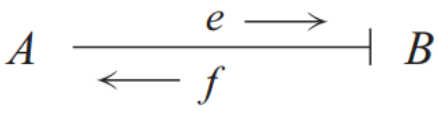

Figure 2.9: The causality stroke (Pedersen and Engja (2014))

2.5 The Park Transform

The Park Transform (Sahm (1979)), also known as the dq0 transform, is a space vector transformation of three-phase time-domain signals from a stationary phase coordinate system (ABC) to a rotating coordinate system (dq0). Simulating a model containing an AC circuit in the ABC

reference frame is very time-consuming on a regular computer since the model's dynamics will be equally fast or faster than the electrical frequency. If the model instead uses a dq0 reference frame rotating at the same frequency as the electrical frequency, the voltages and currents will be constant when the model is in a steady state. So by using the dq0 reference frame instead of the ABC reference frame the amount of simulation time needed will be reduced a lot. Therefore all of the AC parts of the model in this thesis uses the dq0 reference frame.

The equations of the Park transform can be seen in (2.4) and (2.5). The transformation is power-conserving. Active and reactive effect is given by (2.6) and (2.7) respectively.

$$A = \sqrt{\frac{2}{3}} \begin{bmatrix} \cos(\theta) & \cos(\theta - \frac{2}{3}\pi) & \cos(\theta - \frac{4}{3}\pi) \\ -\sin(\theta) & -\sin(\theta - \frac{2}{3}\pi) & -\sin(\theta - \frac{4}{3}\pi) \\ \frac{1}{\sqrt{2}} & \frac{1}{\sqrt{2}} & \frac{1}{\sqrt{2}} \end{bmatrix}$$

$$\mathbf{u}_{d,q,0} = A\mathbf{u}_{a,b,c} \tag{2.4}$$

$$\mathbf{i}_{a,b,c} = A^T\mathbf{i}_{d,q,0} \tag{2.5}$$

$$P = u_d i_d + u_q i_q \tag{2.6}$$

$$Q = -u_d i_q + u_q i_d \tag{2.7}$$

2.6 The synchronous machine

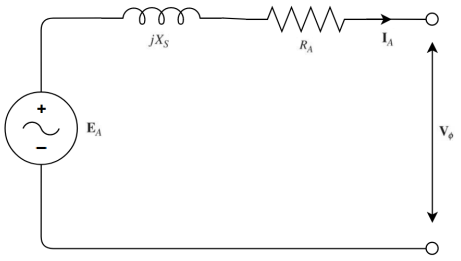

Figure 2.10: Synchronous machine equivalent per phase circuit

A synchronous machine's equivalent per phase circuit (figure 2.10) consists of the induced voltage $\bar{E}_A$, the synchronous reactance X_S, the armature resistance R_A, $\bar{I}_A$ is the current and $\bar{V}_\phi$ is the terminal voltage. The synchronous reactance is comprised of the leakage reactance and the armature reaction. Since the armature resistance usually is much smaller than the synchronous reactance and does not matter for the point in this derivation, it is neglected. The phasor diagram in figure 2.11 is created from the resulting voltage balance of the equivalent circuit (2.8). In the phase diagram, θ is the phase angle between the terminal voltage and the current, while δ is the phase angle between the induced voltage and the terminal voltage.

$$\bar{\mathbf{E}}_A = \bar{\mathbf{V}}_\phi + \mathrm{j}\,\mathrm{X}_S\bar{\mathbf{I}}_A \tag{2.8}$$

By looking at the trigonometric relations in the phasor diagram (figure 2.11), the following relations can be made between δ and the produced active (2.9) and reactive power (2.10). δ is because of this relation also called both the load angle and the power angle of the synchronous machine. More theory about the synchronous machine can be found in Kothari and Nagrath (2010).

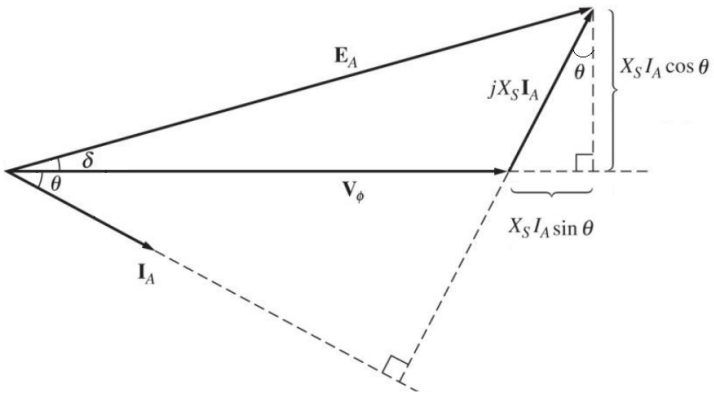

Figure 2.11: Synchronous machine phasor diagram

$$P_\phi = V_\phi I_A \cos\theta = \frac{V_\phi E_A \sin\delta}{X_S} = \tau_e \omega_e - P_{\text{losses}} \tag{2.9}$$

$$Q_\phi = V_\phi I_A \sin\theta = \frac{V_\phi (E_A \cos\delta - V_\phi)}{X_S} \tag{2.10}$$

Where τ_e is the torque applied by the diesel engine, ω_e is the angular velocity of the diesel engine, and P_{losses} accounts for losses in the generator, e.g. friction and windage losses, core losses and copper losses.

2.7 Generator: Active power load sharing

The diesel engine's torque is the generator's power input (2.9); thus it is the diesel engine's governor that controls how much active power the generator produces. There are mainly two types of governor control strategies that are used in the industry: droop and isochronous load sharing (Ådnanes (2003)).

2.7.1 Frequency droop

Frequency droop works such that the reference frequency of the engine is reduced as the load of the engine increases. The reference frequency is calculated by (2.12) and (2.13).

$$D\% = \frac{\omega_{0\%} - \omega_{100\%}}{\omega_{100\%}} * 100 \tag{2.11}$$

$$D = \frac{\omega_{0\%} - \omega_{100\%}}{P_N} \tag{2.12}$$

$$\omega_{ref}(P_d) = \omega_{0\%} - DP_d \tag{2.13}$$

$$e_\omega = \omega_{ref} - \omega_e \tag{2.14}$$

Where D% is the percentage the speed can deviate from the full-load frequency, D is the droop coefficient, $\omega_{0\%}$ is the no-load frequency, $\omega_{100\%}$ is the full-load frequency, ω_{ref} is the governor's reference frequency, P_d is the delivered power and P_N is the rated power.

The greatest advantage of frequency droop is that there does not need to be any communication between the gensets. Each generator will follow their droop curve when the load changes, and stabilise at the steady-state point where the current demand for power is provided. A disadvantage with frequency droop is that the frequency will vary as the load level varies, and thus it is not suitable if the attached equipment is depending on a very stable frequency, or if, e.g. two buses are to be connected. One solution to the problem is to actively modify the droop curve during operation. Another disadvantage is that the transients after a load change might be slow, leading to a period where the gensets will oscillate before settling on the new steady-state point. The droop control might also become unstable if the droop percentage is too low, meaning that a small change in frequency will make the engines go from zero to full load, oscillating endlessly. More information about frequency droop can be found in Wood (2014).

Two example droop curves can be seen in figure 2.12. At the current steady-state of 61.5 Hz, the 5% droop generator delivers 50% of P_N while the 8.33% droop generator delivers 70% of P_N. Both gensets will deliver P_N at 60 Hz which is the full-load frequency, while only the 8.33% droop generator will deliver power if the frequency is above 63 Hz. Thus it is possible to control the load sharing regime by changing the droop coefficients of the individual gensets.

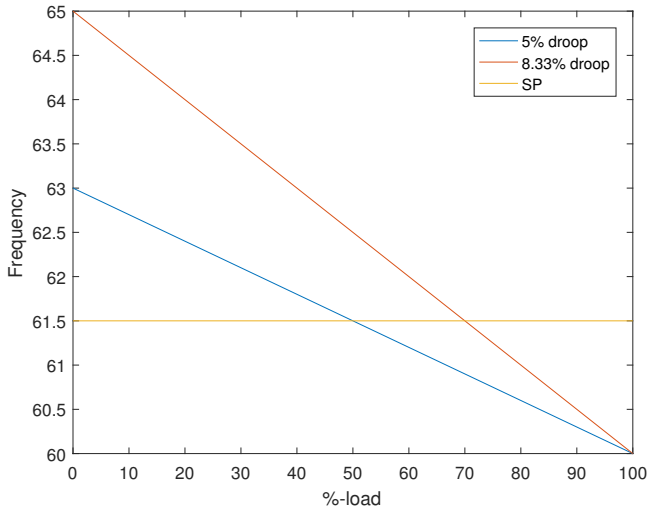

Figure 2.12: Droop curves

The calculated reference frequency ω_{ref} is sent to a PID-controller along with the measured frequency ω_e of the engine. The PID-controller then controls the engine's fuel supply based on the difference e_ω between the reference frequency and the measured frequency (2.14).

2.7.2 Isochronous

Isochronous is a stiff governor control regime compared to frequency droop, where the reference frequency is constant. This means that there needs to be a *load sharing line* connecting all gensets together, if they are connected to the same bus. Without a connection, each genset would try to "fight" the other gensets to get them to run at the same exact frequency as it self. When the load level of all gensets are known, the average power produced can be found (2.15). Each genset has a bias b_i and load gain k_i argument that can be used to achieve asymmetric load sharing. When $\bar{p}$ is known, each genset calculates their own power reference (2.16). The error (2.17) is then used by a PID-controller to adjust the engine's fuel supply.

$$\bar{p} = \frac{1}{n} \sum_{i=1}^{n} \frac{p_i - b_i}{k_i} \tag{2.15}$$

$$p_{\text{ref,i}} = \bar{p} k_i + b_i \tag{2.16}$$

$$e_\omega = K_1(p_{\text{ref}} - p) + K_2(\omega_{ref} - \omega) \tag{2.17}$$

Where p_i, b_i and k_i is the power produced, bias and load gain of genset i respectively and K1 and K2 are constant gains.

An advantage of the isochronous control regime is that the frequency will be close to constant. Some of the disadvantages are that it is more complex to setup compared to frequency droop. The load sharing lines must be connected and disconnected along with the bus tie breakers. It is also a possibility that an error in one genset can spread along the load sharing line and ultimately lead to a common mode failure of all the connected gensets. More information about isochronous control can be found in Wood (2014).

2.7.3 Combined droop and isochronous

A combined droop and isochronous control regime are widely used in island mode operations when the variations of the load are small in comparison with the average load. This setup consists of one genset with isochronous control in parallel with one or more gensets with frequency droop. In operation, the frequency droop gensets will deliver constant power according to its droop curve value at the frequency kept constant by the isochronous genset, while the isochronous genset will handle all of the load variations. Therefore the isochronous genset is often referred to as the swing machine. To change the amount of power that is delivered by the frequency droop gensets, their individual droop curves can be altered during operation. E.g. when a frequency droop genset is connecting to the bus, the no-load frequency is set to the bus frequency, so the genset does not deliver power until the curve is altered to the desired power output afterwards. It is important to dimension the isochronous genset such that it is able to handle any load variation that is likely to occur.

2.7.4 Power management system

A power management system(PMS) knows how much power each genset is generating, and can therefore orchestrate very precise load sharing while keeping the frequency constant. The PMS utilises an adaptive droop algorithm to calculate each engine's speed set-point (2.18). The set-point is sent to the engine's local controller, which is a simple PID-controller acting on the error (2.19).

$$\omega_{sp,i} = \omega_{\text{s}} - \omega_{1,i} + \omega_{2,i} \tag{2.18}$$

$$e_{\text{engine,i}} = \omega_{sp,i} - \omega_i \tag{2.19}$$

The ω_1 and ω_2 terms are governed by (2.20) and (2.21) respectively. ω_1 creates an offset in the set-point, that is positive if the engine's power share is increased and negative if the power share is decreased. ω_2 approaches ω_1 when the engine's power share approaches the set value, and thus nullifies the offset created by ω_1.

$$\dot{\omega}_{1,i} = \frac{((\omega_{\mathrm{s}} - \omega_{1,i})\mathrm{D} * \mathrm{P}_i \sum_{j=1}^{n} \mathrm{L}_j - \omega_{1,i}}{T} \tag{2.20}$$

$$\dot{\omega}_{2,i} = \frac{(\omega_{\mathrm{s}} - \omega_{1,i})\mathrm{D} * \mathrm{L}_i - \omega_{2,i}}{T} \tag{2.21}$$

Where ω_s is the engine's actual set-point, D is the droop parameter, P_i is the power share assigned to generator i ($\sum_{j=1}^{n} P_j = 1$), $\sum_{j=1}^{n} \mathrm{L}_j$ is the sum of the load level on each of the n gensets, L_i is the load level of genset i and T is the time constant of the derivatives low pass filter.

Figure 2.13 shows how ω_1 and ω_2 respond to a change of the power sharing weights. In this scenario, both gensets contribute 50% from the beginning. The weights are then changed 3 times to 0.2/0.8 at t=150 s, 0.5/0.5 at t=200 s and finally to 0.8/0.2 at t=250 s.

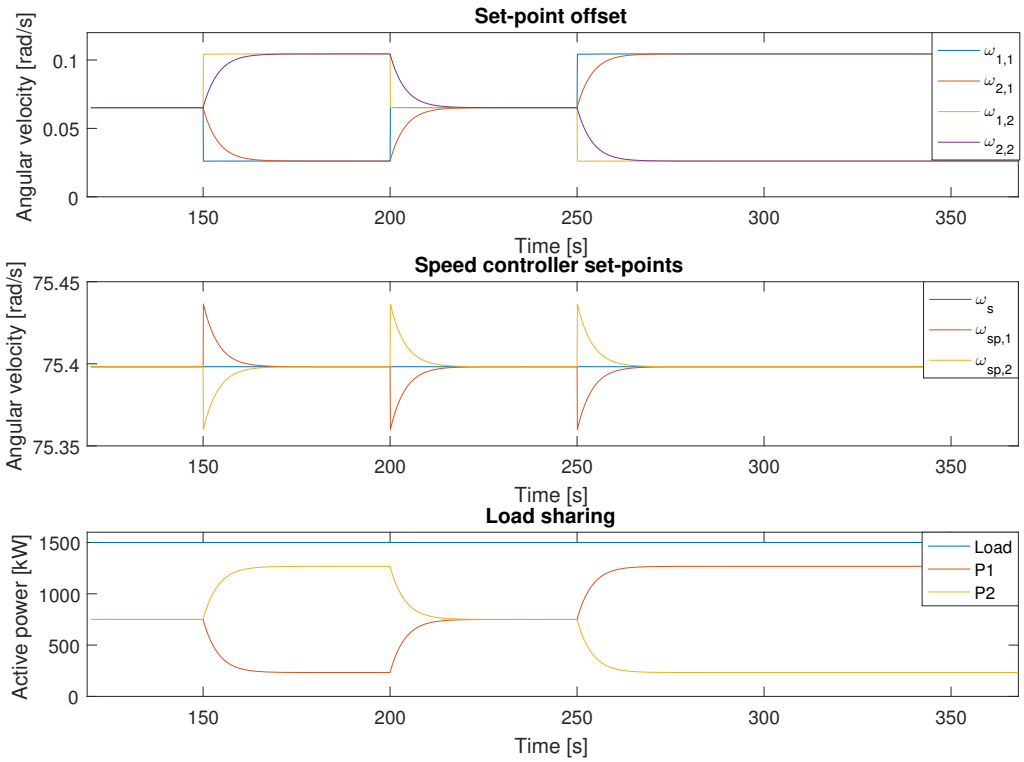

Figure 2.13: PMS - Active load sharing

The active load sharing converges to the new set-point with a 90% rise-time of 8.8 s.

2.8 Generator: Reactive power load sharing

Looking at (2.10), assuming that V_ϕ is constant, it is clear that it is the induced voltage E_A that controls if the machine consumes or delivers reactive power. E_A is a function of the resulting magnetic flux in the air gap between the rotor and stator, which again is a function of the field current in the rotor. Thus it is U_f, the voltage applied to the rotor field windings, that needs to be controlled in order to setup reactive load sharing.

Locally, the genset has an automatic voltage regulator(AVR), that controls U_f with the objective of keeping the amplitude of $\mathbf{u}_{\mathrm{dq}}$ at the voltage set-point. This is done by a simple PID-controller acting on the error in (2.23).

$$V_{\mathrm{rms,i}} = \sqrt{\frac{2}{3}}\sqrt{u_{\mathrm{d,i}}^2 + u_{\mathrm{q,i}}^2} \tag{2.22}$$

$$e_{\mathrm{AVR,i}} = V_{\mathrm{sp}} - V_{\mathrm{rms,i}} \tag{2.23}$$

Where V_{sp} is the voltage set-point.

It is possible to setup reactive power sharing through a similar droop operation as in chapter 2.7.1, by substituting the frequency and active power parameters in (2.12), (2.11) and (2.13) with voltage and reactive power parameters respectively. But as with frequency droop, this leads to that the steady-state voltage will vary according to the reactive load level and the steady-state voltage level must be within ±2.5% of the nominal AC voltage, according to (DNV GL AS (2017)).

To achieve reactive load sharing where the steady-state voltage is kept at the nominal AC voltage, the total amount of reactive load must be known, and thus it is natural to implement it in the PMS. The PMS calculates an offset that is added to the AVR controller's output. The offset is calculated by a PI-controller acting on the error in (2.24).

$$e_{\mathrm{Qoffset,i}} = \mathrm{Qshare}_i \sum_{j=1}^{n} Q_j - Q_i \tag{2.24}$$

Where Qshare_i is the reactive power assigned to genset i ($(\sum_{j=1}^{n} \mathrm{Qshare}_j = 1)$), $\sum_{j=1}^{n} Q_j$ is the total amount of reactive power produced and Q_i is the amount of reactive power produced by genset i.

Thus the total field voltage (2.25) is the sum of the contribution from both AVR and Qoffset calculated by the PMS.

$$u_{\mathrm{f,i}} = \mathrm{AVR}_i + \mathrm{Qoffset}_i \tag{2.25}$$

Figure 2.14 shows how the reactive power sharing scheme responds to changes in the load sharing weights. Both gensets contribute 50% from the beginning. The weights are then changed 3 times to 0.2/0.8 at t=150 s, 0.5/0.5 at t=200 s and finally to 0.8/0.2 at t=250 s.

The reactive load sharing converges to the new set-point with a 90% rise-time of 4.2 s.

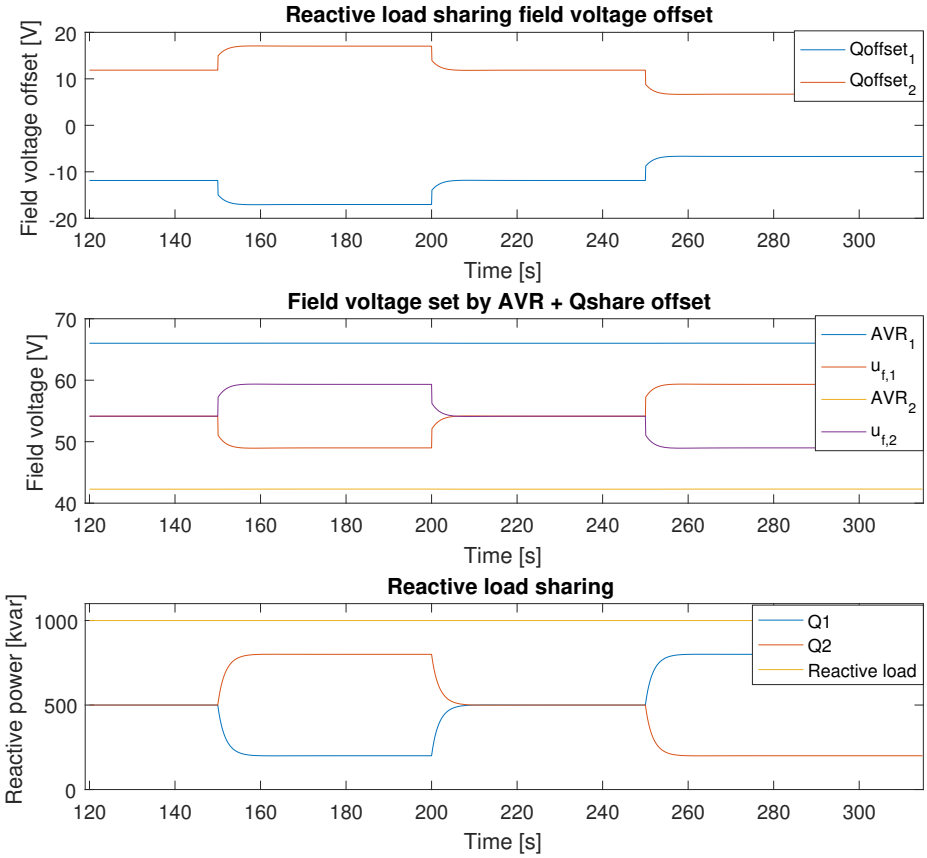

Figure 2.14: PMS - Reactive load sharing

3 Bond Graph Modelling of Load Sharing Model

3.1 Diesel Engine Model

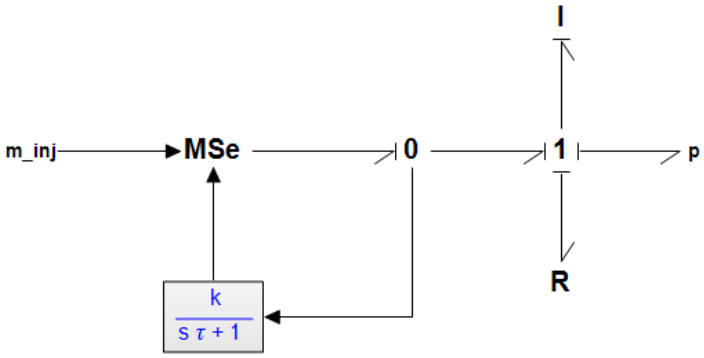

Figure 3.1: Diesel engine bond graph model

The diesel engine model (figure 3.1) consists of three main components. A modulated source effort (MSe), an inertia (I) and a resistance (R). The MSe element calculates how much torque the engine produces, given the injected fuel and specific fuel consumption at the current load level.The constitutive relation for the MSe element is given in (3.3), which depends on (3.2) and (3.1).

$$L = \frac{\omega_e \tau_{\text{shaft}}}{P_{\max}} 100\% \tag{3.1}$$

$$\text{be(L)} = \frac{0.0056L^2 - 0.708L + 207}{1000} \quad [\text{kg/kWh}] \tag{3.2}$$

$$\tau_e(m_{\text{inj}}, L) = \frac{3.6\, m_{\text{inj}}}{4\pi \text{be(L)}} \quad [\text{MNm}] \tag{3.3}$$

Where ω_e is the engine's angular velocity, τ_{shaft} is the measured output torque on the engine's shaft, $P_{\max}$ is the engines maximum continuous rated power, L is the engines load percentage, be(L) is a function that calculates the engines specific fuel consumption at the given load level, $m_{\text{inj}}\,[\frac{\text{kg}}{\text{injection}}]$ is the amount of fuel injected by the motor controller and τ_e is the Torque output by the MSe element.

The I element contains the rotational inertia for both the diesel engine and the generator. Since both of the inertias are linked to the same speed through the shaft, they can be combined, and an algebraic loop is avoided. The constitutive relation for the I element is given in (3.4), where i is the sum of the two inertias.

$$f = \frac{p}{i} \tag{3.4}$$

The R element represents the rotational friction in the engine, and it is modelled as a linear resistance that is proportional to the engine's speed. The constitutive relation for the R element is given in (3.5), where r is the friction constant.

$$e = rf \tag{3.5}$$

The total set of differential equations for the engine is given as

$$\dot{\theta}_e = \omega_e \tag{3.6}$$

$$\dot{\omega}_e = \frac{1}{J_G + J_e}(\tau_e - r\omega_e - \tau_G) \tag{3.7}$$

where θ is the engine's angle and τ_G is the electromagnetic torque of the generator.

The engine's brake specific fuel consumption (BSFC) at nominal speed can be seen in figure 3.2. The consumption goes from 269 g/kWh at 20% load to the minimum of 200 g/kWh at 80% load, which translates to an efficiency rate of 27.9% to 36.9% from fuel specific energy density to energy output at the shaft respectively. (Diesel's fuel specific density is 13.3 kWh/kg)

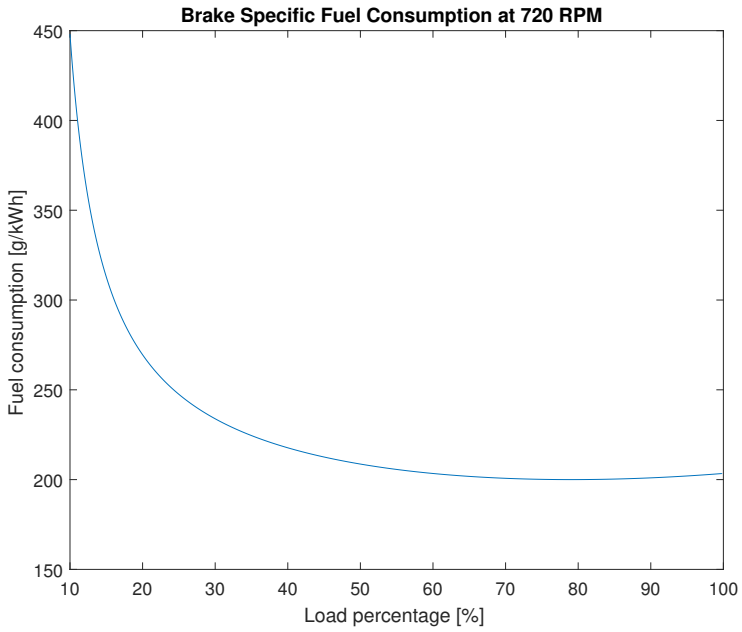

Figure 3.2: The engine's BSFC at 720 RPM

The engine's governor is controlled by the active power load sharing in the PMS as described in chapter 2.7.4, when more than one genset is active.

3.2 Generator Model

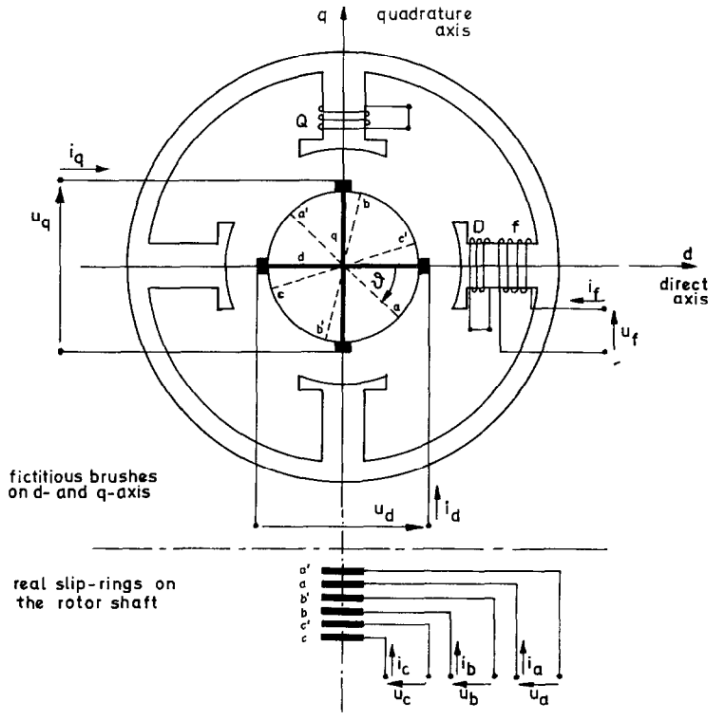

Figure 3.3: The model machine of the two-reaction theory (synchronous machine) (Sahm (1979))

Synchronous machines are widely used both as motors and generators. They are used as motors in industries that consume a lot of reactive power (e.g. large asynchronous machines), to compensate and keep the power factor of the power drawn from the grid in line with the power company's regulations. A synchronous generators output frequency is equal to the shaft speed, therefore they are also the number one choice for alternating current generation when the currents frequency needs to be kept constant.

Based on the stator and rotor equivalent circuits, voltage equations can be obtained in terms of flux linkages and winding resistances by utilising Faraday's and Kirchhoff's laws.

$$\mathbf{U} = \mathbf{Ri} + \frac{d\boldsymbol{\psi}}{\mathrm{dt}} \tag{3.8}$$

Where $\mathbf{U}$ are the voltages, $\mathbf{R}$ is the resistance matrix, $\mathbf{i}$ are the currents and $\boldsymbol{\psi}$ are the flux linkages. If saturation is neglected, the flux linkages are proportional to the currents and can be written as

$$\boldsymbol{\psi} = \mathbf{Li} \tag{3.9}$$

where $\mathbf{L}$ is an inductance matrix containing all of the self- and mutual inductances for the stator and rotor coils. Equation (3.8) and (3.9) can then be combined to form the following differential equation for the flux linkages.

$$\frac{d\boldsymbol{\psi}}{\mathrm{dt}} = \mathbf{U} - \mathbf{RL}^{-1}\boldsymbol{\psi} \tag{3.10}$$

The problem with equation (3.10) is that the $\mathbf{L}$ matrix contains time varying inductances which

are functions of the rotor's position, which means that the inductance matrix would have to be computed at every time step. The time dependency can be removed by applying the Park transform (see chapter 2.5).

After the transformation the $\mathbf{L}$ matrix becomes the diagonal matrix

$$\mathbf{L} = \begin{bmatrix} L_d & 0 & L_{df} & L_{dD} & 0 \\ 0 & L_q & 0 & 0 & L_{qQ} \\ L_{df} & 0 & L_f & L_{fD} & 0 \\ L_{dD} & 0 & L_{fD} & L_D & 0 \\ 0 & L_{qQ} & 0 & 0 & L_Q \end{bmatrix}$$

where L_d, L_q, L_f, L_D and L_Q are constant self-inductances, while L_{df}, L_{dD}, L_{fD} and L_{qQ} are constant mutual inductances. The subscripts d, q, f, D and Q refers to the d-, q-, field-, D- and Q-winding respectively.

The resulting state-space form of the generator model is given in (3.11) and (3.12).

$$\dot{\boldsymbol{\psi}} = -\omega_e \mathbf{D}\boldsymbol{\psi} - \mathbf{R}\mathbf{i} + \mathbf{E}\mathbf{u}_{dq} + \mathbf{b}\mathrm{u}_f \tag{3.11}$$

$$\mathbf{i} = \mathbf{L}^{-1}\boldsymbol{\psi} \tag{3.12}$$

where $\boldsymbol{\psi} = \begin{bmatrix} \psi_d & \psi_q & \psi_f & \psi_D & \psi_Q \end{bmatrix}^T$, $\mathbf{i} = \begin{bmatrix} i_d & i_q & i_f & i_D & i_Q \end{bmatrix}^T$, $\mathbf{u}_{dq} = \begin{bmatrix} u_d & u_q \end{bmatrix}^T$

$$\mathbf{D} = \begin{bmatrix} 0 & -n_p & 0 & 0 & 0 \\ n_p & 0 & 0 & 0 & 0 \\ 0 & 0 & 0 & 0 & 0 \\ 0 & 0 & 0 & 0 & 0 \\ 0 & 0 & 0 & 0 & 0 \end{bmatrix}, \mathbf{E} = \begin{bmatrix} 1 & 0 \\ 0 & 1 \\ 0 & 0 \\ 0 & 0 \\ 0 & 0 \end{bmatrix}, \mathbf{R} = \begin{bmatrix} R_d & 0 & 0 & 0 & 0 \\ 0 & R_q & 0 & 0 & 0 \\ 0 & 0 & R_f & 0 & 0 \\ 0 & 0 & 0 & R_D & 0 \\ 0 & 0 & 0 & 0 & R_Q \end{bmatrix}, \mathbf{b} = \begin{bmatrix} 0 \\ 0 \\ 1 \\ 0 \\ 0 \end{bmatrix}$$

n_p is the generators number of pole pairs, ω_e is the shafts angular velocity and u_f is the field voltage that controls the magnetic field in the rotor.

The electromagnetic torque created by the generator, which is the coupling towards the engine (3.7), is given as (3.13).

$$\tau_G = (\psi_d i_q - \psi_q i_d) n_p \tag{3.13}$$

Marine electrical power systems are not stiff like land-based electrical power systems, meaning that the frequency and voltage levels are not constant. The first genset that comes online sets both the frequency and the voltage, while subsequent gensets have to synchronise to match the frequency and voltage of the grid before the bus tie breaker is closed. Since the genset model derived in (3.11) and (3.12) has current as output, the system has to be solved again with respect to the output voltage.

When (3.11) is rearranged with respect to the output voltage $\mathbf{u}_{dq}$, the resulting equation (3.14) has a derivative causality. This means that the derivative of the d and q flux linkages must be computed.

$$\mathbf{u}_{dq} = \dot{\boldsymbol{\psi}}_{dq} + \omega_e \mathbf{D}_{dq}\boldsymbol{\psi}_{dq} + \mathbf{R}_{dq}\mathbf{i}_{dq} \tag{3.14}$$

where $\boldsymbol{\psi}_{dq} = \begin{bmatrix}\psi_d & \psi_q\end{bmatrix}^T$, $\mathbf{i}_{dq} = \begin{bmatrix}i_d & i_q\end{bmatrix}^T$, $\mathbf{D}_{dq} = \begin{bmatrix}0 & -n_p \\ n_p & 0\end{bmatrix}$ and $\mathbf{R}_{dq} = \begin{bmatrix}R_d & 0 \\ 0 & R_q\end{bmatrix}$.

The state-space is now reduced to the f, D and Q state (3.15), which combined with the $\mathbf{i}_{dq}$ current from the grid, will be used to solve (3.9) with respect to $\boldsymbol{\psi}_{dq}$ and $\mathbf{i}_{fDQ}$.

$$\dot{\boldsymbol{\psi}}_{fDQ} = -\mathbf{R}_{fDQ}\,\mathbf{i}_{fDQ} + \mathbf{b}_{fDQ}\,u_f \tag{3.15}$$

where $\boldsymbol{\psi}_{fDQ} = \begin{bmatrix}\psi_f \\ \psi_D \\ \psi_Q\end{bmatrix}$, $\mathbf{i}_{fDQ} = \begin{bmatrix}i_f \\ i_D \\ i_Q\end{bmatrix}$, $\mathbf{R}_{fDQ} = \begin{bmatrix}R_f & 0 & 0 \\ 0 & R_D & 0 \\ 0 & 0 & R_Q\end{bmatrix}$ and $\mathbf{b} = \begin{bmatrix}1 \\ 0 \\ 0\end{bmatrix}$.

The resulting equations for the d and q flux linkages and field, D and Q currents are given in (3.16) and (3.17). $\mathbf{Z}_{dq}$ and $\mathbf{Z}_{fDQ}$ in (3.18) are derived when (3.9) is solved with respect to $\boldsymbol{\psi}_{dq}$ and $\mathbf{i}_{fDQ}$.

$$\boldsymbol{\psi}_{dq} = \mathbf{Z}_{dq}\begin{bmatrix}\mathbf{i}_{dq} \\ \boldsymbol{\psi}_{fDQ}\end{bmatrix} \tag{3.16}$$

$$\mathbf{i}_{fDQ} = \mathbf{Z}_{fDQ}\begin{bmatrix}\mathbf{i}_{dq} \\ \boldsymbol{\psi}_{fDQ}\end{bmatrix} \tag{3.17}$$

$$\mathbf{Z}_{dq} = \begin{bmatrix}Z_{11} & 0 & Z_{13} & Z_{14} & 0 \\ 0 & Z_{22} & 0 & 0 & Z_{25}\end{bmatrix} \qquad \mathbf{Z}_{fDQ} = \begin{bmatrix}Z_{31} & 0 & Z_{33} & Z_{34} & 0 \\ Z_{41} & 0 & Z_{43} & Z_{44} & 0 \\ 0 & Z_{52} & 0 & 0 & Z_{55}\end{bmatrix} \tag{3.18}$$

where

$$\begin{aligned}
Z_{11} &= \frac{L_D Ld\, L_f - {L_{fD}}^2 Ld - L_D {L_{df}}^2 - {L_{dD}}^2 L_f + 2\, L_{dD} L_{fD} L_{df}}{L_D L_f - {L_{fD}}^2} \\
Z_{13} &= -Z_{31} = \frac{L_D L_{df} - L_{dD} L_{fD}}{L_D L_f - {L_{fD}}^2} \\
Z_{22} &= \frac{-L_qQ^2 + Lq\, L_Q}{L_Q} \\
Z_{25} &= -Z_{52} = \frac{L_qQ}{L_Q} \\
Z_{33} &= \frac{L_D}{L_D L_f - {L_{fD}}^2} \\
Z_{34} &= Z_{43} = -\frac{L_{fD}}{L_D L_f - {L_{fD}}^2} \\
Z_{44} &= \frac{L_f}{L_D L_f - {L_{fD}}^2} \\
Z_{55} &= \frac{1}{L_Q}
\end{aligned}$$

$\boldsymbol{\psi}_{dq}$ is differentiated numerically to get $\dot{\boldsymbol{\psi}}_{dq}$ (3.20), which is the last part needed to solve (3.14). The derivative is low pass filtered through a first order filter (3.19) to reduce noise, which

otherwise may have caused problems in the simulation.

$$\dot{\boldsymbol{\xi}}_{dq} = \frac{1}{T}(\boldsymbol{\psi}_{dq} - \boldsymbol{\xi}_{dq}) \tag{3.19}$$

$$\dot{\boldsymbol{\psi}}_{dq} = \frac{1}{T}(\boldsymbol{\psi}_{dq} - \boldsymbol{\xi}_{dq}) \tag{3.20}$$

A bond graph implementation of the generator with current and voltage output can be seen in figure 3.4 and figure 3.5 respectively. All states, and the derivative of $\dot{\boldsymbol{\psi}}_{dq}$ in the voltage output scenario, is computed inside the I-elements. The inertia of the generator is added inside the diesel engine bond graph (see chapter 3.1).

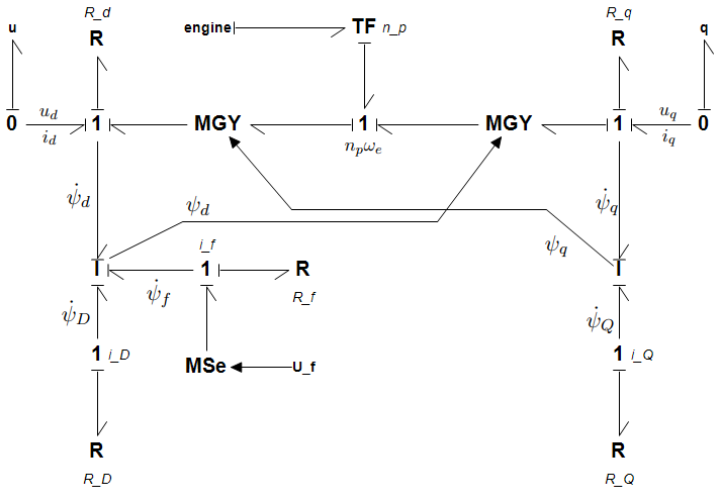

Figure 3.4: Generator bond graph model with current output

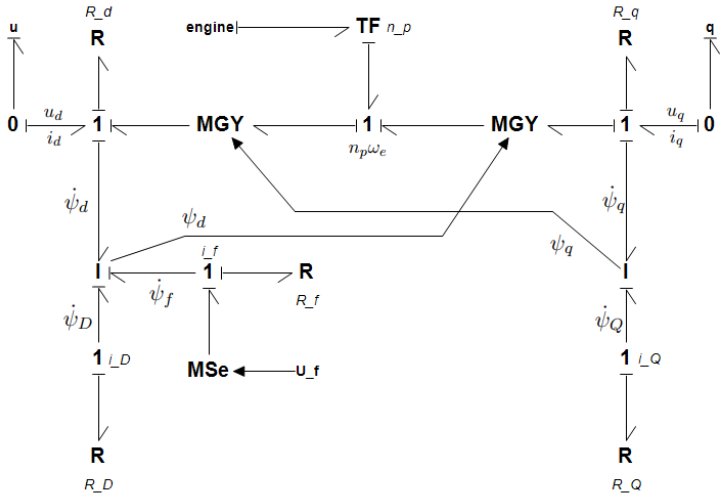

Figure 3.5: Generator bond graph model with voltage output

The generator's AVR and reactive power sharing offset is setup as described in chapter 2.8, where the offset, which is controlled by the PMS, only is applied when more than one genset is active. The final genset-model, which is used in the simulations, contains two gensets and a PMS. The model is not made by the author, so the reader is advised to read Skjong and Pedersen (2017) for more information about e.g. PMS genset synchronisation logic.

3.3 Battery Model

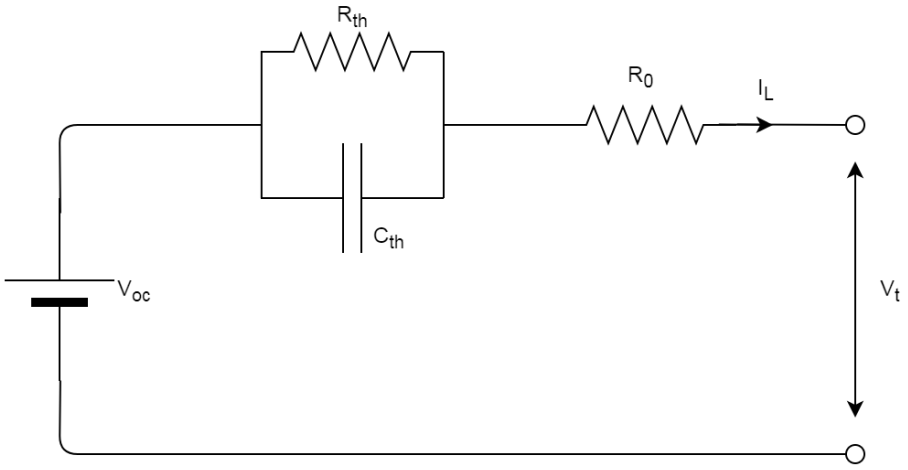

Figure 3.6: Battery cell Thevenin equivalent circuit

As discussed in chapter 2.2.2, a Thevenin equivalent battery circuit (figure 3.6) is sufficient to investigate the potential power savings of marine hybrid power operations. The parameters in the Thevenin equivalent circuit are the open circuit voltage (OCV) V_{OC}, the battery's internal resistance R_0 and a parallel RC circuit with a resistance of R_{th} and a capacitance of C_{th}. All battery parameter values (table 3.1) are supplied by the department of Energy Storage at ABB Marine, and are based on a battery cell with Lithium-nickel-manganese-cobalt (NMC) chemistry.

B_{Ah}	64 Ah
R_0	$0.8m\Omega$
R_{th}	$0.2m\Omega$
τ_B	15 s

Table 3.1: Battery cell parameters [ABB Marine]

Where τ_B is the battery's time constant given by $\tau_B = C_{\text{th}}R_{\text{th}}$. The parameters vary significantly with temperature and will drift over time as the battery ages. This model however assumes that the battery has proper cooling, and that the C-rates are kept within bounds of what the cooling system can handle. The model's purpose is to investigate possible benefits trough a case study and not for simulating a battery's degradation of time, thus the aging effects are not included. It is therefore found acceptable to keep the battery parameters constant.

The measured OCV (figure 3.7) is linearised as (3.23) for values of state of charge (SoC) greater than 10%. As discussed in chapter 2.2.1, discharging the battery below 10% will damage it permanently and reduce the battery's expected lifetime. Thus the linearization covers the whole working interval of the battery. These cells can be over charged to 4.2V but should be kept below 4.15 V (104.2% SoC) to achieve an acceptable lifetime.

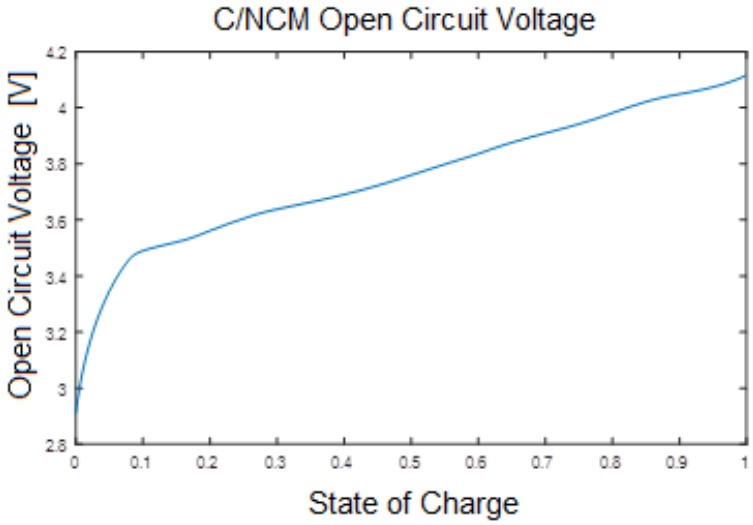

Figure 3.7: Battery open circuit voltage [ABB Marine]

SoC (3.22) represents the percentage of charge left in the battery and is found by integrating the battery's current flux (3.21) and then looking at the percentage difference of (3.21) compared to the total amount of charge when the battery is full B_{Ah}.

$$B_{\text{state}} = \frac{\int_0^t I_L dt}{3600} \tag{3.21}$$

$$\text{SoC} = \frac{B_{\text{Ah}} - B_{\text{state}}}{B_{\text{Ah}}} \tag{3.22}$$

$$V_{\text{oc}} = (3.42 + 0.7 * \text{SoC}) \tag{3.23}$$

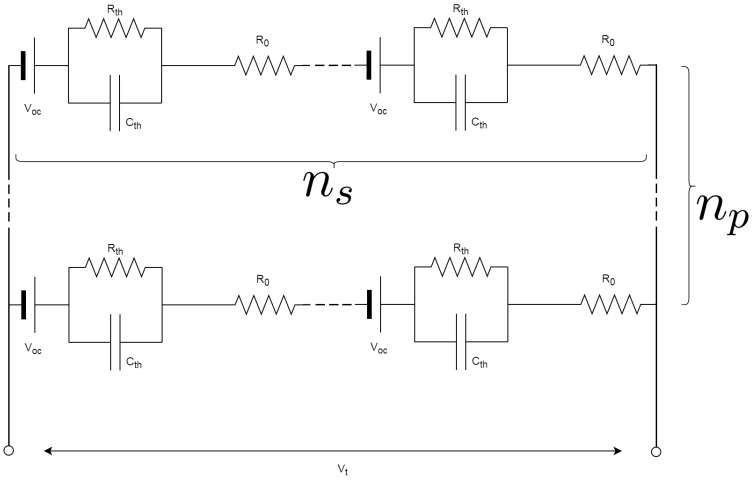

Figure 3.8: Battery pack Thevenin equivalent circuit

Battery cells are wired in series to achieve the voltage level necessary to work at the voltage levels of the intended environment. The resulting string of batteries is often referred to as a battery pack. The battery pack's capacity can be increased by connecting several strings of battery cells in parallel. Figure 3.8 shows the total setup of a battery pack, where n_s is the number of battery cells in each string and n_p is the number of parallel battery strings.

The battery pack's total terminal voltage and capacity are given as (3.24) and (3.25) respectively.

$$V_{\text{oc,pack}} = V_{\text{oc}} n_s \tag{3.24}$$

$$B_{\text{Ah,pack}} = B_{\text{Ah}} n_p \tag{3.25}$$

The battery cells inside the pack are super positioned into one Thevenin equivalent circuit. Resistances in series can be replaced with an equivalent resistance with the size of the sum of all resistances, $R_{\text{tot,series}} = R_1 + ... + R_n$, or $R_{\text{tot,series}} = nR_1$ if all resistances are equal. Resistances in parallel can be replaced with an equivalent resistance with the size as the reciprocal of the sum of reciprocals like $\frac{1}{R_{\text{tot,parallel}}} = \frac{1}{R_1} + ... + \frac{1}{R_n}$, or $R_{\text{tot,parallel}} = \frac{R_1}{n}$ if all resistances are equal. By combining these two rules, the resulting value for R_0 and R_{th} are given like (3.26) and (3.27) respectively. The battery's time constant, τ_B, is not affected by how many battery cells are connected in series and parallel. Thus the resulting value of C_{th} is given by (3.28).

$$R_{0,\text{pack}} = R_0 \frac{n_s}{n_p} \tag{3.26}$$

$$R_{\text{th,pack}} = R_{\text{th}} \frac{n_s}{n_p} \tag{3.27}$$

$$C_{\text{th,pack}} = \frac{\tau_B}{R_{\text{th,pack}}} \tag{3.28}$$

With all the parameters of the battery pack in place, the terminal voltage of the pack can be set up like (3.29), where V_{th} is the voltage drop over the RC loop, given by the differential equation (3.30).

$$V_{\text{t,pack}} = V_{\text{oc,pack}} - V_{\text{th,pack}} - R_{0,\text{pack}} I_L \tag{3.29}$$

$$\dot{V}_{\text{th,pack}} = \frac{I_L}{C_{\text{th,pack}}} - \frac{V_{\text{th,pack}}}{\tau_B} \tag{3.30}$$

The resulting bond graph implementation can be seen in figure 3.9.

The battery pack's power capacity in different configurations are given in table 3.2. The numbers were extracted from simulation, by discharging at 1 C from 90% SoC to 10% SoC, which is the total SoC range the battery pack should operate in to preserve the battery's SoH. The two numbers represent the power delivered to the load and the internal power drawn from the battery respectively, i.e. the difference is the power dissipated in the internal resistance.

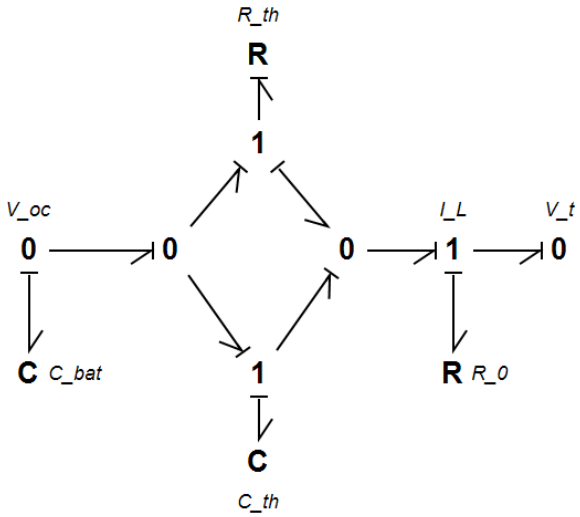

Figure 3.9: Battery pack bond graph model

	$n_s = 200$	$n_s = 250$
$n_p = 1$	36/38.6 kWh	45/48.3 kWh
$n_p = 2$	78.8/82.4 kWh	99.3/103/kWh
$n_p = 4$	163.2/170 kWh	205.6/212.6 kWh
$n_p = 8$	332/345.4 kWh	418.2/431.8 kWh

Table 3.2: Battery pack usable power capacity at 1 C discharge

3.3.1 DC/DC Converter Model

A bidirectional DC/DC converter makes the PMS able to control the battery pack's power flow by boosting or reducing the voltage level of the bus. The converter is represented by an MTF-element in the bondgraph model, where the bus sets the voltage and the battery sets the current. The losses in the converter are accounted for by the efficiency parameter η_{dcdc}. The constitutive relation for the converter's output voltage is given in (3.31), while the current output to the bus is given by (3.32) when $P_{\text{bat}} >= 0$ and (3.33) when $P_{\text{bat}} < 0$.

$$V_{\text{dcdc}} = m\, V_{\text{bus}} \tag{3.31}$$

$$i^{+}_{\text{bus}} = m\, i_{\text{dcdc}}\, \eta_{\text{dcdc}} \tag{3.32}$$

$$i^{-}_{\text{bus}} = \frac{m\, i_{\text{dcdc}}}{\eta_{\text{dcdc}}} \tag{3.33}$$

Where m is a signal from the PMS. To calculate the value of m needed to make the battery supply or consume a given amount of power, the relation in (3.34) is used. (3.34) i real as long as $V^2_{\text{bat}} > 4P_{\text{bat}}R$. $V_{\text{bat}} > 690V$, $R < 0.2\Omega$ and $P_{\text{bat}} < 1MW$, which makes m real in all the scenarios of this thesis.

$$m = \frac{V_{\text{bat}} + \sqrt{V^2_{\text{bat}} - 4P_{\text{bat}}R}}{2V_{\text{bus}}} \tag{3.34}$$

(3.34) is developed by assuming that there is a known resistance R between the battery and the converter (figure 3.10), and that both the battery (V_{bat}) and converter (V_{dcdc}) voltage is known. R could be e.g. a small inserted resistance and/or the resistance in the wire between the battery and the converter. The resistance can be estimated through an adaptive estimator by monitoring the voltages and current.

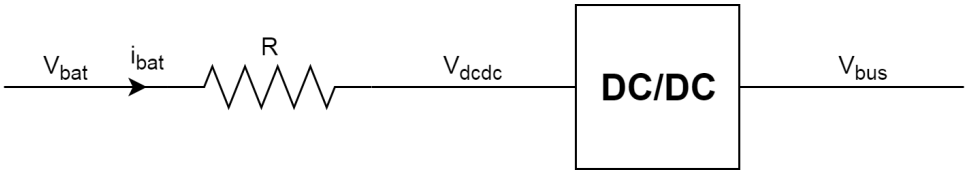

Figure 3.10: DC/DC converter diagram

When the value of the resistance between the battery and converter is known, (3.34) is found by inserting the (3.35) and (3.31) into (3.36) and then solving for m.

$$i_{\text{bat}} = \frac{V_{\text{bat}} - V_{\text{dcdc}}}{R} \tag{3.35}$$

$$P_{\text{bat}} = V_{\text{dcdc}}\, i_{\text{bat}} \tag{3.36}$$

In order to ensure that the gensets' and battery pack's operations are stable in the model, the battery pack needs to have a minimum amount of resistance to dampen the system. Trough simulation testing, this resistance has been found to be $R_{\text{b,tot}} = 0.06\Omega$ and $R_{\text{b,tot}} = 0.11\Omega$ for the $n_s = 200$ and $n_s = 250$ battery string versions respectively. To handle this issue, the resistance R in (3.34), is set to be the remaining resistance to reach the minimum target if the battery's internal resistance R_0 is too small, which it always is for $n_p > 1$. Further more, in this model, R_0 and R are combined into one resistance to avoid an algebraic loop in the battery model.

The resistance in the battery pack is used as a bus-tie breaker when the battery pack is not active. This is done by setting the resistance to 10 GΩ, which in practice means that the current going through will be negligible.

The control strategies for P_{bat} are discussed thoroughly in chapter 4.

3.4 AC/DC Converter Model

The AC/DC converter transforms the dq0 AC signal to a DC signal. Power conservation is applied to create the constitutive laws for the converter, e.g. power on the DC side is equal to the power on the DQ side, minus the converter's losses. The losses are accounted for by an efficiency factory η_{acdc}. Since there is no such thing as reactive power in a DC grid, the only reactive power that needs to be considered is the reactive power consumed by the converter. The amount of reactive power drawn is set up as a function of the converters power factor (PF) as in (3.39).

The dq0 currents can then be calculated by rearranging (2.6) and (2.7), where the values for P are given by (3.37) when $P_{DC} >= 0$ and (3.38) when $P_{DC} < 0$.

The AC/DC converter provides voltage to the DC side and currents to the dq0 side. Thus the constitutive laws for the AC/DC converter is given in (3.40) and (3.41) respectively. The converter is implemented in the bond graph model as a TF-element.

$$P_{DC}^{+} = VI\eta_{\text{acdc}} \tag{3.37}$$

$$P_{DC}^{-} = \frac{VI}{\eta_{\text{acdc}}} \tag{3.38}$$

$$Q = -|P_{DC}|\sqrt{\frac{1}{PF^2} - 1} \tag{3.39}$$

$$V = \sqrt{\frac{2}{3}}\sqrt{u_d^2 + u_q^2} \tag{3.40}$$

$$\mathbf{i}_{d,q} = \frac{1}{u_d^2 + u_q^2}\begin{bmatrix} u_d & u_q \\ u_q & -u_d \end{bmatrix}\begin{bmatrix} P_{DC} \\ Q \end{bmatrix} \tag{3.41}$$

3.5 Load Profile

The load profile used in case study two is based on a 75 tonnes load cycle for the MACGREGOR GLE7526-MLC-6030-2 crane. The data for the load cycle, supplied by Grieg Star, can be seen in table 3.3. The load from the active cranes are added on top of a constant hotel load of 375 kW. The cycle is repeated if the simulation exceeds the time of one cycle. Some of the cycle's events has a random timing aspect, such that each cycle pass will be unique and the effects of different load variations can be examined.

Phase	Duration (s)	Power (kW)
1 Random start	0-30	0
2 Load on	45-85	20
3 Hoisting 15 m	45	372
4 Luffing in & hoisting 5 m	14	475
5 Slewing 75°	27	80
6 Lowering 10 m	27	-212
7 Load off	10-20	20
8 Hoisting 5 m & slewing 75°	15	125
9 Luffing out & lowering 15 m	30	-89
Exit or start over from step 2		

Table 3.3: Load cycle

An example of a load cycle with one active crane can be seen in figure 3.11.

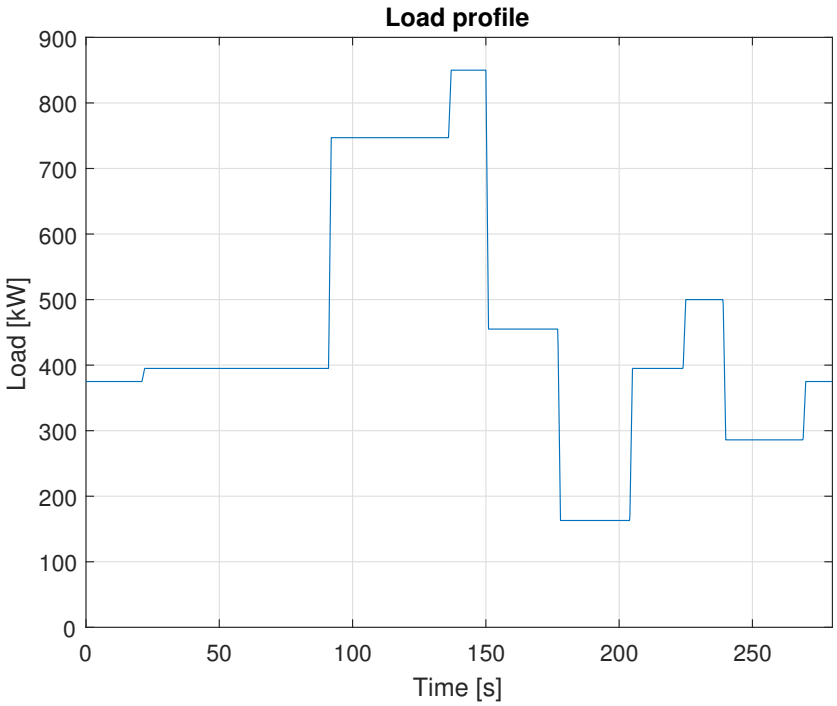

Figure 3.11: Load cycle with hotel load and one crane

The load profile is applied through a DataFromFile block in 20-sim. The DataFromFile block reads the load profile from a csv-file, which is generated by the Python code in appendix C. The load signal from the DataFromFile block is then sent to an equation block, which acts as the load. The load block calculates the currents that is needed to draw the specified power, based on the voltage level on the grid, trough (3.41), except that P_{DC} is replaced with the signal from the DataFromFile block. The amount of reactive power drawn is set up as a function of the loads power factor (PF) as in (3.39), where the loads PF is assumed to be 0.8.

If the battery is not connected during a simulation, the load activates load shedding by saturating the signal from the DataFromFile block with a lower limit. In reality, this is done by e.g. activating large pumps to burn off the energy. The amount of energy burnt off is calculated by integrating the difference between the load and the minimum genset limit when the load is below the limit.

4 Control strategies

Each of the control strategies in the following sections returns $P_{\text{g,sp}}$, which is the requested power from the gensets, to the battery logic function (BLF). The BLF determines which one of the different control strategies that are active, and then sets the battery pack's set-point $P_{\text{b,sp}}$ to the difference between the total load P_{L} and $P_{\text{g,sp,active}}$ as in (4.1).

$$P_{\text{b,sp}} = P_{\text{L}} - \text{sat}(P_{\text{g,sp,active}}, P_{\text{g,min}}, P_{\text{g,max}}) \tag{4.1}$$

The value of $P_{\text{g,sp,active}}$ is saturated to ensure that it is between the lower ($P_{\text{g,min}}$) and upper ($P_{\text{g,max}}$) limit of the genset's power limits. The saturation function used in this chapter, sat(value,min,max), takes 3 arguments. The first is the value to be saturated, the second is the lower bound, and the third is the upper bound.

if $\text{BT}_b == 1$ **then**
  $P_{\text{blf,sp}} = P_{\text{b,sp}}$
else
  $P_{\text{blf,sp}} = 0$
  $P_{\text{blf,offset}} = P_{\text{blf,f}}$
end if

$P_{\text{blf,sp}}$ is set to the output from the active control strategy if the battery pack's bus-tie breaker BT_b is closed ($\text{BT}_b == 1$), and zero otherwise. An offset $P_{\text{blf,offset}}$ is updated with the filtered output's current value, to ensure that the output is zero whenever the bus-tie breaker is open or the switching algorithm is changing from one control strategy to another. $P_{\text{blf,sp}}$ is then filtered (4.2) to avoid algebraic loops, where T_f is the filter's time constant.

$$P_{\text{blf,f}} = \int \frac{P_{\text{blf,sp}} - P_{\text{blf,f}})}{T_f}\,\text{dt} \tag{4.2}$$

As discussed in chapter 2.2.1, the battery pack's power input and output must be bounded in order to maintain the battery pack's state of health. The battery pack's maximum input (4.3) and output (4.4) current is given by the set C-rate limits.

$$i_{b,in,max} = -B_{\text{Ah,pack}} * C_{in,max} \tag{4.3}$$
$$i_{b,out,max} = B_{\text{Ah,pack}} * C_{out,max} \tag{4.4}$$

Where $B_{\text{Ah,pack}}$ (3.25) is the battery pack's total amount of ampere hours.

The battery pack's maximum input and output power limits are then found through (4.5) and (4.6) respectively. The values are filtered to avoid algebraic loops, where T_f is the filter's time constant.

$$P_{b,in,max} = \int \frac{V_b i_{b,in,max} - P_{b,in,max}}{T_f} \tag{4.5}$$

$$P_{b,out,max} = \int \frac{V_b i_{b,out,max} - P_{b,out,max}}{T_f} \tag{4.6}$$

The saturated final output, which is sent to (3.34) in the DC/DC converter, is then given as (4.7).

$$P_{\mathrm{b,dcdc}} = \mathrm{sat}(P_{\mathrm{blf,f}} - P_{\mathrm{blf,offset}}, P_{b,in,max}, P_{b,out,max}) \tag{4.7}$$

4.1 Average Power Control

The average power control's objective is, as the name implies, to make the gensets handle the average load, while the battery pack handles all transients. This control strategy aims at minimising the amplitude of the gensets transients, and thus reducing the wear and tear on the genset. This control strategy requires that the battery pack has enough capacity to handle largest transients for the time it takes the average filter to catch up.

$$P_{\mathrm{avg}} = sat\left(\int \frac{(P_L + P_c) - P_{\mathrm{avg}}}{T_{\mathrm{avg}} T_{\mathrm{d}}}, P_{\mathrm{g,min}}, P_{\mathrm{g,max}} \right) \tag{4.8}$$

$$P_{\mathrm{c}} = K_{\mathrm{c}}(\mathrm{SOC_{sp}} - \mathrm{SOC}) \tag{4.9}$$

The average power is calculated by (4.8), where P_L is the power consumed by the load and T_{avg} is the time constant of the average filter, as long as the calculated average is close to the gensets actual load. P_c (4.9) is a proportional controller, with gain K_c, which adds a bias to the genset load to prevent the battery pack's SoC to diverge too far from the given set-point, $\mathrm{SOC_{sp}}$. The integral is saturated to stay within the bounds of the gensets capability limits.

A dynamic time constant T_d (4.10) is used in (4.8) to ensure that the average power filter quickly returns to the actual genset load in the event of a power spike in the gensets' delivered power. Such power spikes occur when the battery pack does not have the capacity to provide the difference between P_L and P_{avg}. An offset P_{offset} (4.11) is subtracted from the control strategy's final output , to prevent integrator windup when P_{avg} exceeds the genset's power limits.

Both T_d and P_{offset} are filtered with a time constant T_f to avoid sudden step changes in the average filter.

$$T_{\mathrm{d}} = \int \frac{T_{\mathrm{d,sp}} - T_{\mathrm{d}}}{T_f} \tag{4.10}$$

$$P_{\mathrm{offset}} = \int \frac{P_{\mathrm{offset,sp}} - P_{\mathrm{offset}}}{T_f} \tag{4.11}$$

The set-points for the T_d and P_{offset} filters are set in the logic below.

if $|P_g - P_{\mathrm{avg}}| > P_{\mathrm{dl}}$ **then**

$P_{\text{offset,sp}} = P_g - P_{\text{avg}}$
$T_{\text{d,sp}} = 0.1$
else
if $|P_L - P_{\text{avg}}| > P_{\text{lsl}}$ **then**
$T_{\text{d,sp}} = 0.5$
else
$T_{\text{d,sp}} = 1$
end if
end if

Where P_{dl} is the drop limit and P_{lsl} is the load step limit. When $|P_g - P_{\text{avg}}| > P_{\text{dl}}$, either the battery pack or the genset has exceeded its capacity. To fix the first case, the dynamical time constant T_d is made ten times faster and to fix the latter, the offset is updated. The load step limit P_{lsl} is set such that the dynamical time constant T_d is made two times faster when the load changes rapidly, to make sure that the average is kept in the area where the battery pack has enough capacity to handle the transients, and thus reducing the probability that the drop limit will be triggered.

The control strategy's output back to the BLF is given as (4.12).

$$P_{\text{g,sp}} = P_{\text{avg}} - P_{\text{offset}} \tag{4.12}$$

4.2 Power Rate Limit Control

Power rate limit control's objective is to keep the magnitude the of gensets' power transient rates below a set threshold. This means that the battery pack will only contribute when the load transients are faster than the threshold. Keeping a bound on the transients felt by the gensets will reduce wear and tear which in turn will lead to reduced maintenance costs. The advantage with this strategy compared to the average load control strategy is that it requires much less battery capacity, and thus is cheaper to implement. The capacity can be smaller since the genset follows tightly, and thus reduces the magnitude of the transients the battery pack has to handle.

The genset's rate of change ($\dot{P}_{\text{g}}$) is given by (4.13).

$$\dot{P}_{\text{g}} = \frac{P_{\text{L}} + P_{\text{c}} - P_{g,sp}}{T_f} \tag{4.13}$$

Where P_c is the same battery charging bias used in (4.9), P_L is the power consumed by the load, $P_{\text{g,sp}}$ is the gensets power set-point from the previous time step and T_f is a time-constant to speed up the derivative.

The logic below acts as an anti-windup, by setting $\dot{P}_{\text{g,sp}}$ to zero if $\dot{P}_{\text{g}}$ is negative while $P_{\text{g,sp}}$ is below the gensets lower power limit ($P_{\text{g,min}}$), and likewise if $\dot{P}_{\text{g}}$ is positive while $P_{\text{g,sp}}$ is above the gensets upper power limit ($P_{\text{g,max}}$). If none of the above contitions apply, $\dot{P}_{\text{g,sp}}$ is set to $\dot{P}_{\text{g}}$, but the value is saturated by $\pm\dot{P}_{\text{g,max}}\, n_{\text{g}}$, where $\dot{P}_{\text{g,max}}$ is the value of each genset's max rate of change and n_{g} is the number of active gensets.

if $(P_{\text{g,sp}} < P_{\text{g,min}}$ **and** $\dot{P}_{\text{g}} < 0)$ **or** $(P_{\text{g,sp}} > P_{\text{g,max}}$ **and** $\dot{P}_{\text{g}} > 0)$ **then**
$\dot{P}_{\text{g,sp}} = 0$
else

$\dot{P}_{\mathrm{g,sp}} = \mathrm{sat}(\dot{P}_{\mathrm{g}}, -\dot{P}_{\mathrm{g,max}}\, n_{\mathrm{g}}, \dot{P}_{\mathrm{g,max}}\, n_{\mathrm{g}})$
end if

$\dot{P}_{\mathrm{g,sp}}$ is integrated to get the gensets' power set-point $P_{\mathrm{g,sp}}$ (4.14), which is then returned to the BLF.

$$P_{\mathrm{g,sp}} = \int \dot{P}_{\mathrm{g,sp}}\, \mathrm{dt} \tag{4.14}$$

4.3 Dynamical Limit Control

Dynamical limit control's objective is to keep the genset working within a defined upper and lower power limit. To reduce the gensets' fuel consumption, these limits are set such that they bound the area where the gensets operate most efficiently. Most engines' efficiency rating does not increase much above the most optimal load percentage, typically $\sim 80\%$ load, so the upper limit does not contribute to much fuel saving directly. The upper limit's purpose is to give the battery pack some space to use all the energy it receives while the load is below the lower limit. Without the upper limit, the battery pack would over charge and never contribute with any energy. Power rate limit control is active on the genset while it is within the interval of the dynamical limits.

A set of dynamical limits is designed to ensure that the battery pack is never charged or discharged too much. The lower and upper dynamical limits are governed by the P-controllers in (4.15) and (4.16) respectively.

$$P_{\mathrm{g,dyn,L}} = K_{\mathrm{p,L}}\,(\mathrm{SOC_U} - \mathrm{SOC}) \tag{4.15}$$
$$P_{\mathrm{g,dyn,U}} = K_{\mathrm{p,U}}\,(\mathrm{SOC_L} - \mathrm{SOC}) \tag{4.16}$$

Where $\mathrm{SOC_L}$ and $\mathrm{SOC_U}$ are the lower and upper SoC limit parameters respectively. $K_{p,L}$ and $K_{p,U}$ are proportional gains that tunes the behaviour of the dynamical limits. When the SoC exceeds the interval [$\mathrm{SOC_L}$, $\mathrm{SOC_U}$], the limits will start to adjust the load window the genset should handle, and thus forcing the SoC back into the interval.

The two logic sections below determines the lower $P_{\mathrm{g,opt,L}}$ and upper $P_{\mathrm{g,opt,U}}$ power limit of the gensets. As long as the battery pack's SoC is between the lower and upper SoC limit, $P_{\mathrm{g,opt,L}}$ and $P_{\mathrm{g,opt,U}}$ are simply the limits set by the operator. Namely $P_{\mathrm{g,L}}$ and $P_{\mathrm{g,U}}$. If the battery pack's SoC is greater than $\mathrm{SOC_U}$, $P_{\mathrm{g,opt,L}}$ will start to decrease and if the battery pack's SoC is less than $\mathrm{SOC_L}$, $P_{\mathrm{g,opt,L}}$ will start to increase. $P_{\mathrm{g,opt,L}}$ and $P_{\mathrm{g,opt,L}}$ are bounded by the genset's minimum and maximum power output respectively.

if $\mathrm{SOC} > \mathrm{SOC_U}$ **then**
$P_{\mathrm{g,opt,L}} = \max([n_g P_{\mathrm{g,L}} + P_{\mathrm{g,dyn,L}}, P_{\mathrm{g,min}}])$
else
$P_{\mathrm{g,opt,L}} = n_g P_{\mathrm{g,L}}$
end if
if $\mathrm{SOC} < \mathrm{SOC_L}$ **then**
$P_{\mathrm{g,opt,U}} = \min([n_g P_{\mathrm{g,U}} + P_{\mathrm{g,dyn,U}}, P_{\mathrm{g,max}})])$
else
$P_{\mathrm{g,opt,U}} = n_g P_{\mathrm{g,U}}$
end if

Where n_g is the number of active gensets.

The next logic section determines how much the battery pack has to contribute to keep the genset running inside the set interval. The battery pack will go into a charging state as long as the total load is lower than $P_{\mathrm{g,opt,U}}$ and the SoC value is lower than $\mathrm{SOC_L}$. The charging power is set to the difference of the power consumed by the load and $P_{\mathrm{g,opt,U}}$. If the difference exceeds $P_{b,in,max}$ (4.5), $P_{b,in,max}$ is used instead.

if $P_{\mathrm{L}} > P_{\mathrm{g,opt,U}}$ **then**
  $P_{\mathrm{b}} = P_{\mathrm{L}} - P_{\mathrm{g,opt,U}}$
else if $P_{\mathrm{L}} < P_{\mathrm{g,opt,U}}$ **and** $\mathrm{SOC} < \mathrm{SOC_L}$ **then**
  $P_{\mathrm{b}} = \max\{P_{\mathrm{bat,in,max}}, P_{\mathrm{L}} - P_{\mathrm{g,U}}\}$
else if $P_{\mathrm{L}} < P_{\mathrm{g,opt,L}}$ **then**
  $P_{\mathrm{b}} = P_{\mathrm{L}} - P_{\mathrm{g,opt,L}}$
else
  $P_{\mathrm{b}} = 0$
end if

Now when the battery pack's contribution is set, the gensets' power rate of change can be found as in (4.17), where P_L is the power consumed by the load, $P_{\mathrm{g,sp}}$ is the gensets' power set-point in the previous time step and T_f is a time-constant to speed up the derivative. Again $\dot{P}_{\mathrm{g,sp}}$ is saturated within the gensets maximum rate of change $\dot{P}_{\mathrm{g,max}}\, n_g$, where $\dot{P}_{\mathrm{g,max}}$ is the maximum rate of change one genset can handle, and n_g is the number of gensets active, before it is integrated (4.18) and sent to the BLF.

$$\dot{P}_{\mathrm{g,sp}} = \frac{P_L - P_b - P_{\mathrm{g,sp}}}{T_f} \tag{4.17}$$

$$P_{\mathrm{g,sp}} = \int sat(\dot{P}_{\mathrm{g,sp}}, -\dot{P}_{\mathrm{g,max}}\, n_g, \dot{P}_{\mathrm{g,max}}\, n_g)\,\mathrm{dt} \tag{4.18}$$

5 Case Study

5.1 Case 1: Verify control strategies

Three individual simulations will be executed to decide which of the three control strategies (described in chapter 4) that are best fit to be used in the thesis' main case study (chapter 5.2).

5.1.1 Case setup

The simulations will feature a genset in parallel with a battery pack and a load. The load profile (5.1) for all three load tests consist of a constant term, a slowly varying load and noise, applied through a first-order hold.

$$P_L = C_L + G_L(G_{L,A}, G_{L,f}) + G_N(G_{N,A}, G_{N,f}) \tag{5.1}$$

Where G_L and G_N are Gaussian white noise. The arguments of G_L and G_N are the amplitude and frequency of the white noise respectively. G_L represents a slowly varying load, while the faster G_N is added as noise to test the robustness of the control method. The parameters' values are listed in table 5.1.

C_L	500 kW
$G_{L,A}$	250 kW
$G_{L,f}$	0.05 Hz
$G_{N,A}$	100 kW
$G_{N,f}$	1.0 Hz

Table 5.1: Load profile parameters

The load test simulation configuration consists of one genset and a battery pack with $n_p = 4$ strings of $n_s = 250$ cells, i.e. 256 Ah and 205.6 kWh (see (3.25) and table 3.2). All other model parameters are listed in appendix B. The battery pack's C-rate that is plotted during these simulations is defined in the following way: The battery receives power from the grid when the C-rate is positive.

The Runge-Kutta 4 integration method is chosen as the solver with a solver time step $\Delta t = 0.2$ ms. The simulation events are listed in table 5.2.

Time [s]	**Event**
0	Genset starts
50	Load is connected
150	Battery is connected
150	Control initiated
500	Simulation ends

Table 5.2: Load test simulation events

5.1.2 Load test: Average Power Control

The control objective of the average power control is, as stated in chapter 4.1, to make the genset handle the average load, while the battery pack handles all of the fast transients. The average load P_{avg} in figure 5.1 is responsive to the load variations before the battery is connected, caused by $|P_g - P_{\text{avg}}| > P_{\text{dl}}$ ($P_{\text{dl}} = 10kW$), making the filter up to ten times faster than normal. As soon as the battery connects at t=150 s, the genset settles down to the average load, and the average load returns to its normal speed. The filter speeds up at the relatively large load transients from t=285 s to t=330 s, caused by $|P_{\text{load}} - P_{\text{avg}}| > P_{\text{lsl}}$ ($P_{\text{lsl}} = 250kW$), which makes the filter up to two times faster. The $\dot{P}_g$ plot in figure 5.2 confirms that the genset's job is made much more comfortable where $\max(|\dot{P}_g|) < 25$ kW/s.

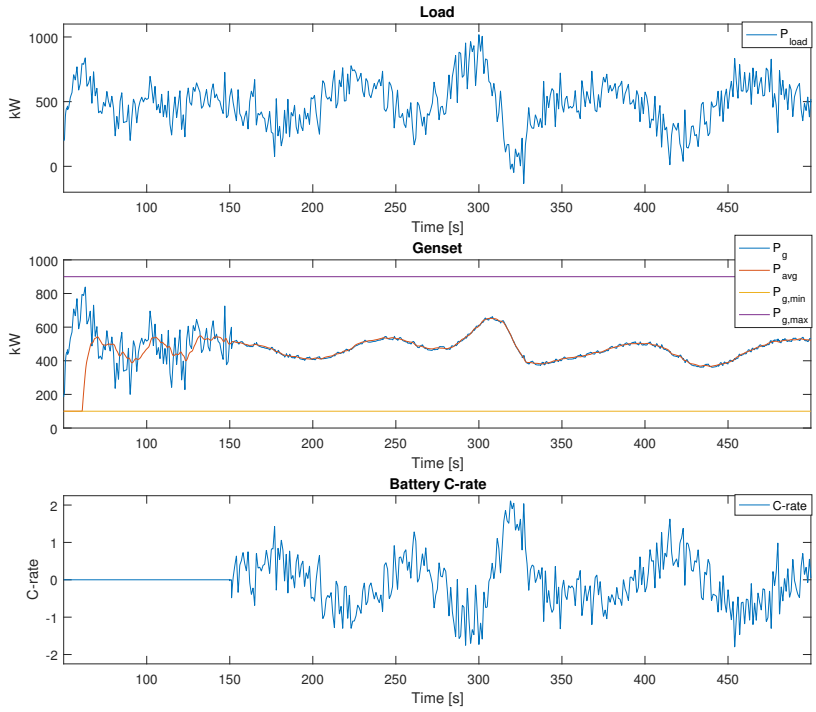

Figure 5.1: Average power control: Load test simulation pt1

The C-rate plot in figure 5.1 shows the contours of the load variations after t=150 s, as expected. The min and max C-ratings in this simulation are 2.1 and -1.8 respectively, which is well within the limits of the battery's capability. Since the load profile's mean is constant, the SoC plot in figure 5.2 is expected to oscillate close to the starting point, which it does, given that the simulation time is long enough to even out local variations. The charging offset P_c, in the same figure, is as expected looking like an inverted version of the SoC plot. The values are pretty insignificant in this simulation since the SoC values are so close to the optimal SoC value of 75%.

The average power control's overall performance is good in this given scenario. The most crucial parameter is the battery pack's capacity to handle the largest load transients. The battery pack's depth of discharge (DoD) is bound to be fairly small, given that the load transients around the average load most likely will be equally positive and negative over a large period of time. Even if there are some local deviations, the charging offset will ensure that the SoC never deviates too much from the optimal level. The shallow DoD means that brief periods of C-rate above ± 2 can be accepted, without affecting the battery pack's lifetime too much. Thus the load profile can have larger transients without the need of increasing the size of the battery pack.

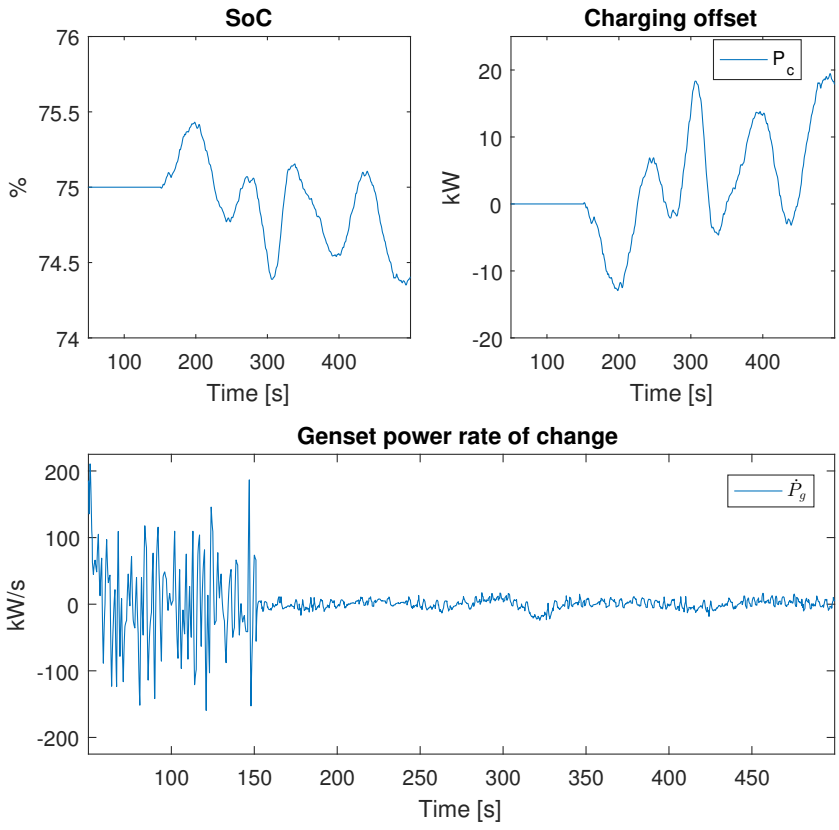

Figure 5.2: Average power control: Load test simulation pt2

5.1.3 Load test: Power Rate Limit Control

The control objective of the power rate limit control is, as stated in chapter 4.2, to keep the magnitude of the gensets' power transient rates below a set threshold. The threshold in this simulation is set to $|\dot{P}_g < 50|$ kW/s. The $\dot{P}_g$ plot in figure 5.4 shows that the threshold is kept successfully after the battery is connected at t=150 s. As expected, the genset load (P_g in figure 5.3) varies much more with this control strategy, compared to the average load strategy, but the load variations are smoothed out by the battery pack. This reduced the wear and tear of the genset while keeping the battery size to a minimum.

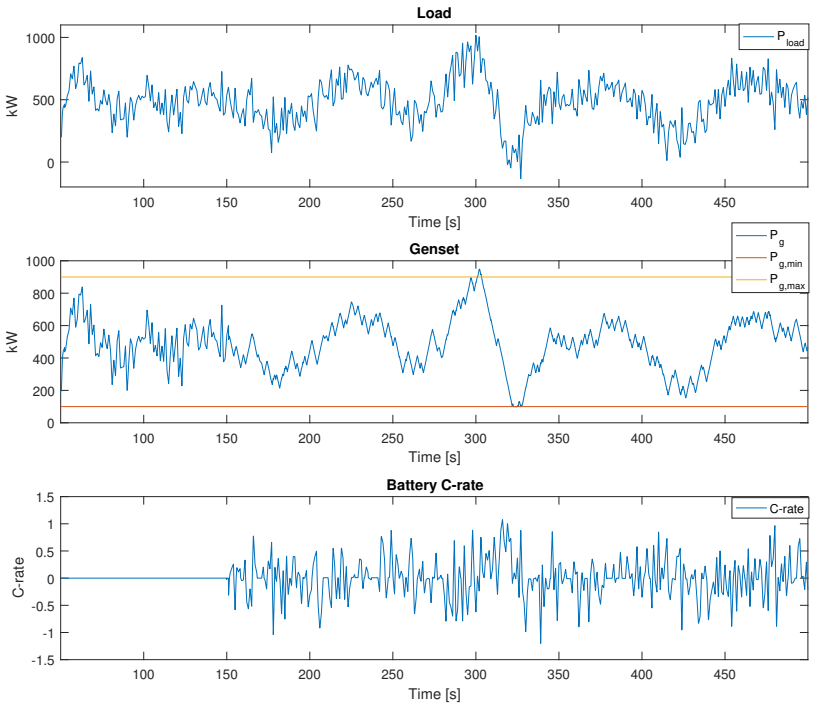

Figure 5.3: Power rate limit control: Load test simulation pt1

The C-rate plot in figure 5.3 shows that the min and max C-rates are -1.2 and 1.1 respectively, and the DoD is minimal (SoC plot in figure 5.4). Thus the battery could have been reduced to half of the size and still manage to do the job. The SoC variations are so small, that the charging offset P_c has little to no effect in this simulation.

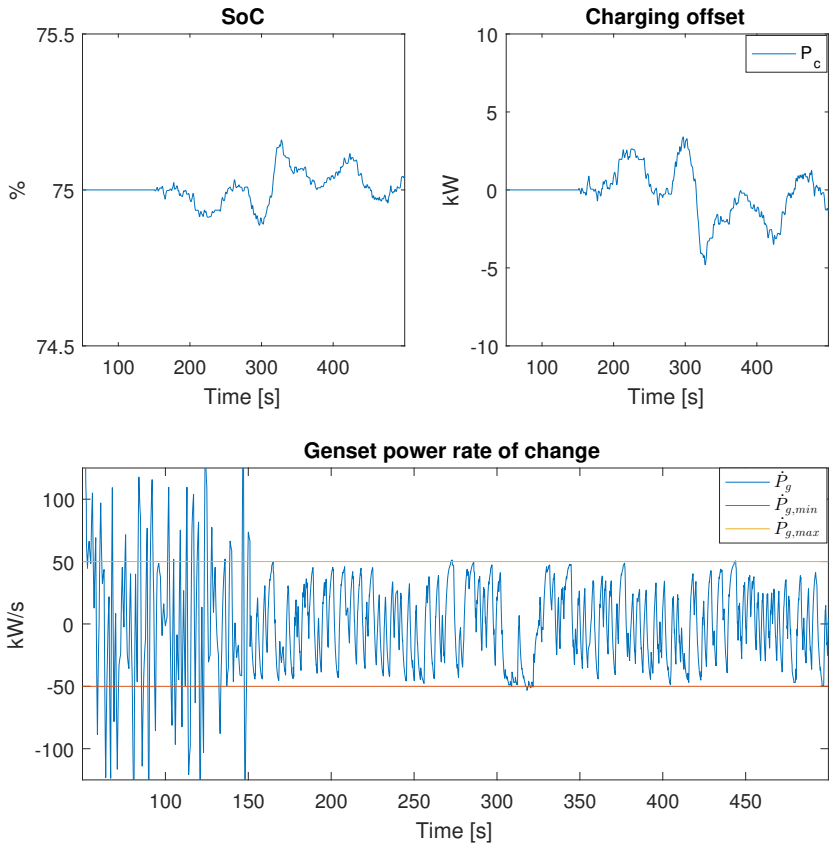

Figure 5.4: Power rate limit control: Load test simulation pt2

5.1.4 Load test: Dynamical Limit Control

Before the results of this load test are presented, a special simulation is conducted in order to demonstrate how the dynamical limits behave. The loads and parameters used in this demonstration are purposefully chosen such that the limits' behaviour is demonstrated in one simulation. The simulation events are listed in table 5.3 and the dynamical limit control parameters are listed in table 5.4.

Time [s]	**Event**
0	Genset starts
50	Load is connected, 500 kW
70	Load step up to 900 kW
150	Battery is connected
150	Control initiated
800	Load step up to 1100 kW
850	Load step down to 900 kW
900	Load step down to 500 kW
1100	Load step down to 100 kW
1800	Load step up to 500 kW
2000	Simulation ends

Table 5.3: Simulation events: Dynamical limits demonstration

$\mathrm{SOC_L}$	78%
$\mathrm{SOC_U}$	72%
$P_{\mathrm{g,L}}$	400 kW
$P_{\mathrm{g,U}}$	700 kW

Table 5.4: Parameters: Dynamical limits demonstration

The demonstration results can be seen in figure 5.5. The genset settles at the optimum max limit once the battery pack is connected. $P_{\mathrm{g,opt,U}}$ starts increasing when the SoC reduces to under $\mathrm{SOC}_L = 72\%$, which makes the genset handle more of the power, and thus preventing that the battery pack's SoC drops too much. If the load should increase above $P_{\mathrm{g,max}}$, the battery will step in, as seen at t=800 s. The genset enters the charging state when the load drops below $P_{\mathrm{g,opt,U}}$ at t=900 s. Thus the genset continues to deliver $P_{\mathrm{g,opt,U}}$ until the battery is above $\mathrm{SOC}L$. $P_{\mathrm{g,opt,L}}$ starts to decrease when the SoC exceeds $\mathrm{SOC}_U = 78\%$. If the SoC continues to rise, $P_{\mathrm{g,opt,L}}$ will settle at the $P_{\mathrm{g,min}}$, to prevent the battery pack's SoC from over charging. It is assumed that the power profile would never be below the $P_{\mathrm{g,min}}$ for a long period of time, so the battery pack will still receive the difference between the load and $P_{\mathrm{g,min}}$, but it is deemed very unlikely that this will lead to the battery pack over charging. The $P_{\mathrm{g,opt,L}}$ will not increase until the SoC has reduced, even though the load goes $P_{\mathrm{g,opt,L}}$. Power rate limit control is active when the load is in between the upper and lower limits, to reduce wear and tear, which explains the short spikes of C-rate e.g. at t=1800 s.

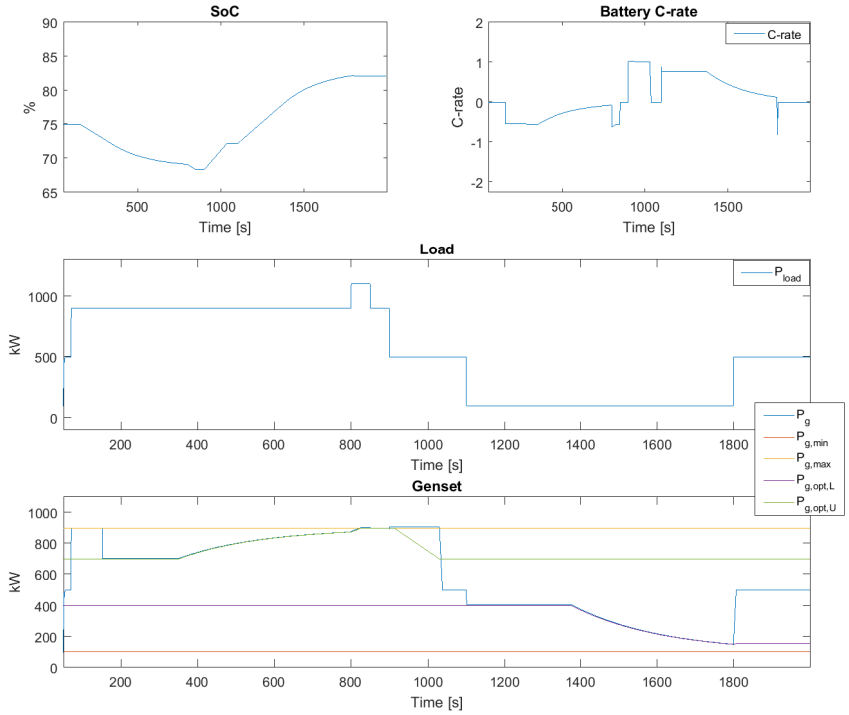

Figure 5.5: Dynamical limit control: Demonstration of dynamical limits

The control objective of the dynamical limit control is, as stated in chapter 4.3, to make the gensets work within their most efficient load interval, to reduce fuel consumption. The dynamical limit control parameters are listed in table 5.4.

$\mathrm{SOC_L}$	78%
$\mathrm{SOC_U}$	72%
$P_{\mathrm{g,L}}$	400 kW
$P_{\mathrm{g,U}}$	750 kW

Table 5.5: Parameters: Dynamical limits demonstration

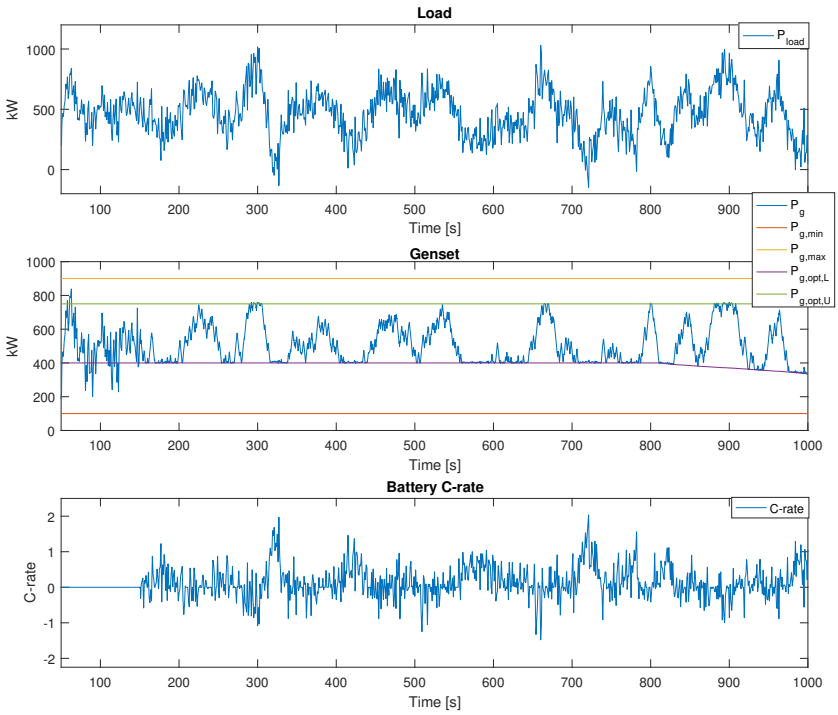

Figure 5.6: Dynamical limit control: Load test simulation pt1

Looking at the plot of P_g in figure 5.6, P_g is kept within $P_{\text{g,opt,L}}$ and $P_{\text{g,opt,U}}$ at all times when the battery pack is active. As the SoC (figure 5.7) exceeds SOC_U at t=810 s, $P_{\text{g,opt,L}}$ starts to decrease, as expected. The genset's power rate of change is kept between the limits of $|\dot{P}_g < 50|$ kW/s as seen in the $\dot{P}_g$ plot of figure 5.7. Since the load profile's mean of 500 kW is below the mean of the interval $[P_{\text{g,L}}, P_{\text{g,U}}]$, which is 575 kW, the SoC level is rising, as seen in the SoC plot in figure 5.7. Thus the limits should be modified in order to optimise the dynamic limit control strategy for this given scenario.

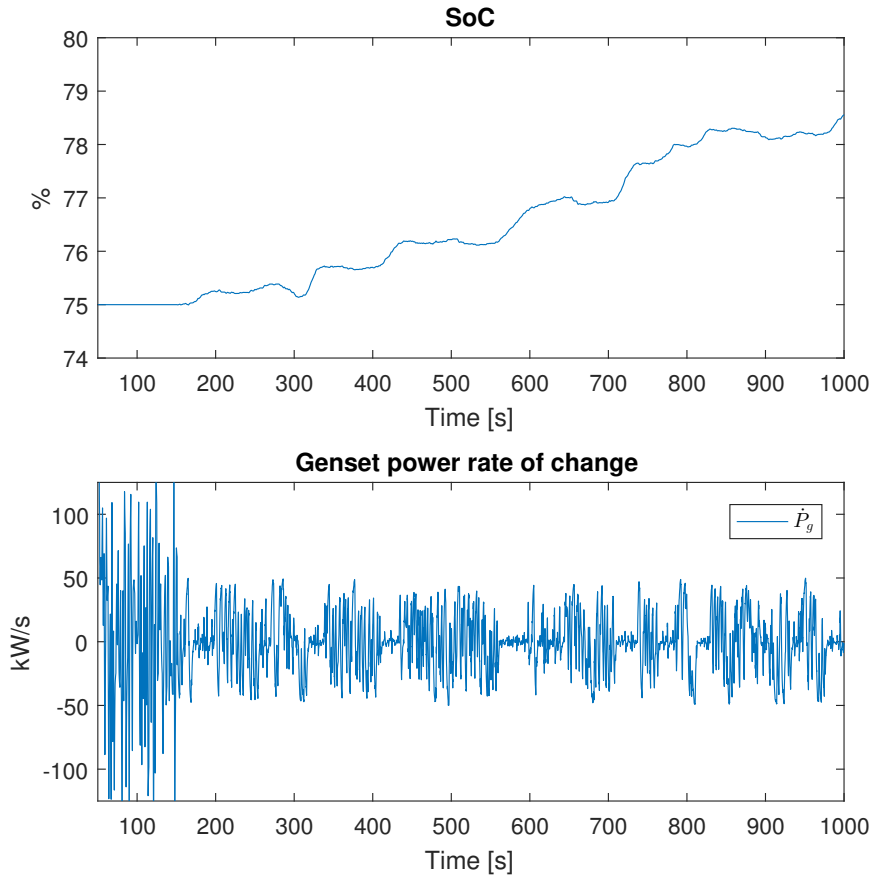

Figure 5.7: Dynamical limit control: Load test simulation pt2

5.1.5 Discussion

The upper limit in the dynamical limit control strategy does not contribute directly to much reduction of fuel consumption since most engines' BSFC does not increase much above their most effective point of $\sim 80\%$. The reason it is included is to maintain the balance between the battery pack's input and output power. Without the upper limit, this control strategy would only charge the battery. Another solution, if two or more gensets are needed to power the load, is to start or stop one of the gensets as the battery pack's SoC reaches a lower or upper limit respectively. As for the lower limit, it is important that the battery pack has enough capacity to handle the power when the load is at its lowest. E.g. if the lower limit is set to run each genset at 50% during an operation where there are regenerative sources active, like the cranes in the Grieg Star case, the total influx of power to the battery may become very large in the extremes. If the battery's capacity is too small at any point, the gensets' load will drop to avoid damaging the battery.

A turbocharged combustion engine does not respond well to step loads. In order to provide enough torque to handle the load, the governor will inject more fuel than there is air in the cylinder to combust, resulting in an incomplete combustion. This happens because of the turbocharger's need to build up speed before it can deliver the amount of air needed. The phenomenon is often referred to as turbo lag, and it is easy to see when it occurs by the black smoke coming out of the exhaust, which is mostly unburnt carbon. See (Garrett (2000)) for more info on black smoke and the combustion process. The black smoke is bad for both the engine's fuel efficiency and the environment, so it should be avoided if possible. All three control strategies will minimise the occurrence of black smoke, be reducing the power rate of change of engine. The average load control reduces the rate of change to a minimum, while the power rate limit control active in the two other strategies limits the rate of change to a figure set by the operator, so it can be adapted according to the engine's capabilities.

5.2 Case 2: Electrical Crane Load Study

5.2.1 Case setup

The objective of this case is to investigate how much the fuel consumption can be reduced in a typical crane operation on board one of Grieg Stars open hatch carriers, with a focus on active power load sharing. The load profile used is generated from the load cycle described in chapter 3.5.

Running the operation without a battery pack requires two active gensets for one or two cranes and three active gensets for three or four cranes. The battery pack described in the section below can supply the maximum power of a genset at a C-rate of 2.34. The biggest possible load in a cycle with two cranes is 1325 kW, so the battery pack will work within the ± 2 C interval during the whole simulation, which is well within the operational limits with regards to the battery packs SoH. Thus the plan is to run two simulations. One with two active gensets and one with one active genset assisted by a battery pack. Figure 5.8 shows a single line diagram of the case setup.

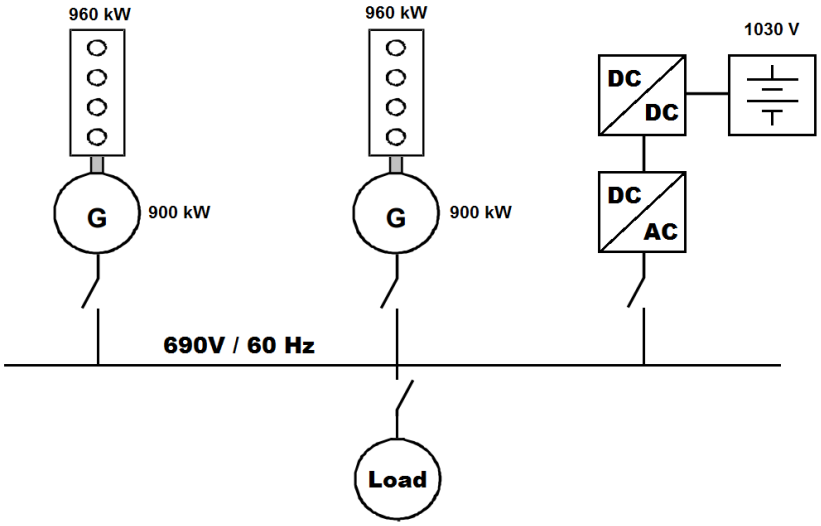

Figure 5.8: Single line diagram of case setup

The control strategy used to control the battery pack in this case study is a mix of the dynamical limit control and average load control strategies. The average load control is implemented to minimise the wear and tear on the genset, and thus minimising the maintenance costs. The dynamical limit control is implemented to minimise fuel consumption, by keeping the genset running at an optimum load level. So to sum up: The genset will handle the average load while the load is within the optimal min and max limit, and produce the optimum min and max in other cases. The limits will move if the load average, related to the optimal limits, is off by so much that the SoC diverges too far from the optimum level. The charging offset is active, to prevent the SoC to diverge from the optimum level.

The parameters for the dynamical limits can be seen in table 5.6. The $P_{g,U}$ limit is forced to 600 kW at t=9000 s to ensure that the SoC returns to the initial state of 75%. This means that the battery pack's contribution is a null sum game, such that there is no need to compensate for a change in the battery pack's energy balance when analysing the power consumption results. All other values can be found in appendix B.

$\mathrm{SOC_L}$	80%
$\mathrm{SOC_U}$	60%
$P_{\mathrm{g,L}}$	500 kW
$P_{\mathrm{g,U}}$ t <= 9000 s	800 kW
$P_{\mathrm{g,U}}$ t > 9000 s	600 kW
K_c	20 kW
$K_{\mathrm{p,L}}$	50 kW/%
$K_{\mathrm{p,U}}$	50 kW/%

Table 5.6: Parameters: Dynamical limit control

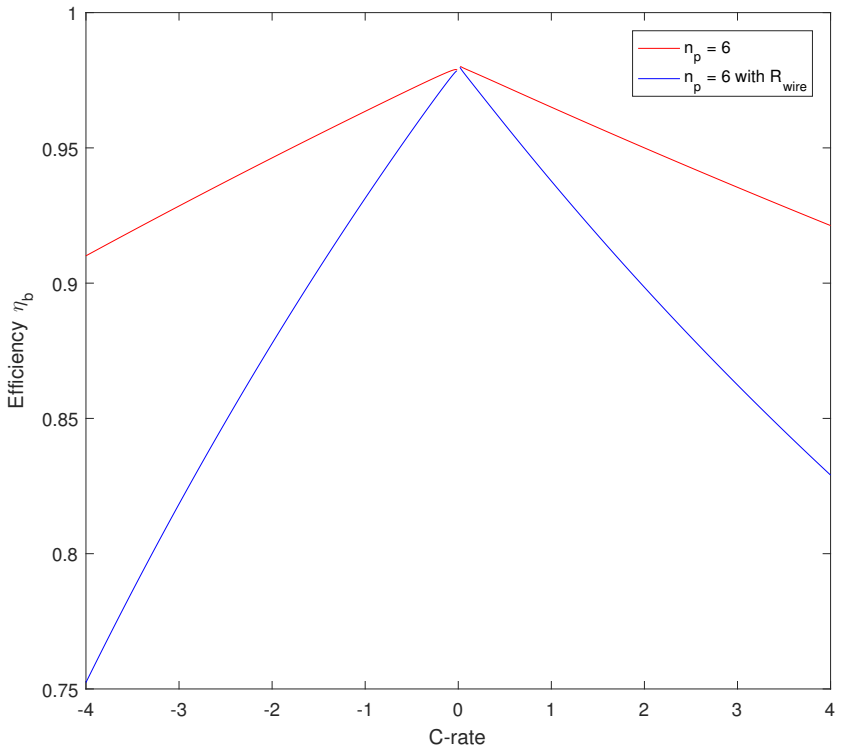

Figure 5.9: Battery pack efficiency at 80% SoC

The battery pack used in this study consists of $n_p = 6$ parallel strings of $n_s = 250$ battery cells in series, i.e. a battery pack with 384 Ah/362 kWh and a voltage range of 872.5 V to 1012.5 V, which can deliver 290 kWh in the operating SoC range from SoC=10% to SoC=90%, minus losses to e.g. internal resistance and converters.

The battery pack's efficiency can be seen in figure 5.9. As mentioned in chapter 3.3.1, the $n_s = 250$ string battery pack must have a minimum total resistance of 0.11Ω to ensure stability, so the remaining resistance is added as wire and DCDC converter resistance (R_{wire}). Thus the battery pack's efficiency in this load case differs much from the efficiency of the real battery pack. E.g. the efficiency from power into power out, including losses in the DC/DC and the AC/DC converter, at a C-rate of 1, has an actual efficiency of up to $0.963 * 0.965 = 0.929$, while the model including R_{wire} has an efficiency of $0.938 * 0.9312 = 0.873$. There are other losses in a real battery pack, e.g. cooling, but the overall efficiency will probably be in the upper part of the interval of [0.873, 0.929]. Thus the results with regard to fuel reduction in this load case will be very conservative.

5.2.2 Results

Since all values are identical for both gensets after they are synchronised, while running 50/50 load sharing on both active and reactive power, there will be plotted values for only one of the gensets in the results. The simulation with two gensets without battery pack assistance and the simulation with the battery pack assisted genset are from now on referred to as simulation one and simulation two respectively.

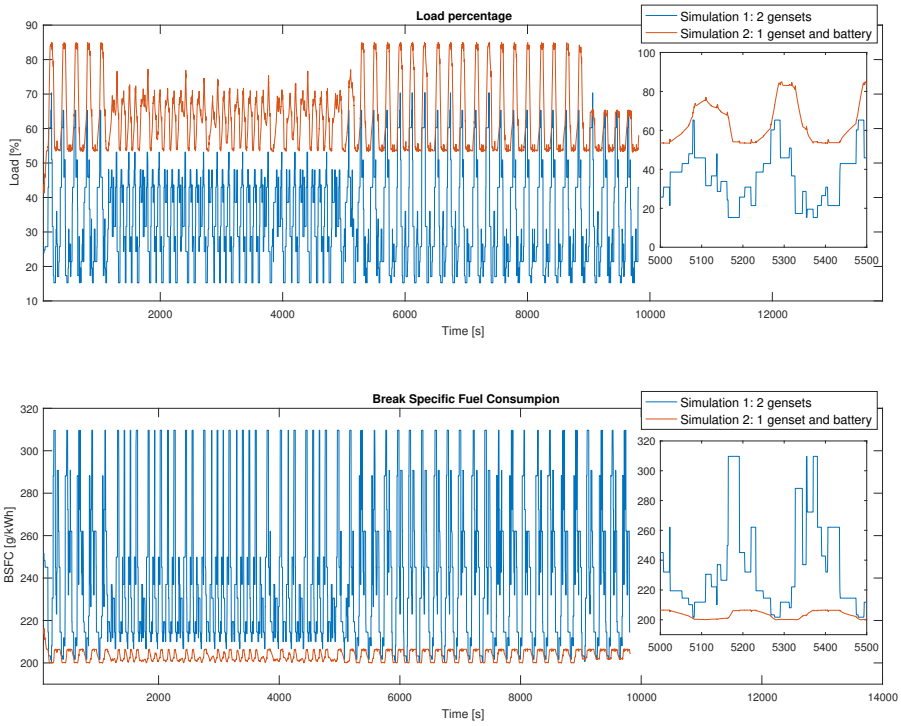

Figure 5.10: Genset load percentage and BSFC

Looking at the load percentage and BSFC plots in figure 5.10, it is clear that the genset in simulation 1 has a much smoother load profile than the gensets in simulation two. The genset in simulation one has a max power rate of change of $\pm 20kW/s$, while the gensets in simulation two has a global max power rate of change of $\pm 250kW/s$ and local average max power rate of change of $\pm 100kW/s$. Which means less wear and tear and thus less maintenance costs related to running the case in simulation one compared to simulation two. The largest contributor to the reduction of maintenance costs in simulation one is the fact that only one genset is running. This means that the effective machine hour rate is the half of that in simulation two. Thus the total reduction in maintenance costs while simulation one is running compared to simulation two will be higher than 50%.

The battery pack's average efficiency in this case study was $\eta_b = 0.891$. The efficiency was calculated by looking at the total amount of energy in and energy out of the ac/dc converter. Converted to the optimal case where R_wire is zero, using the factors found in chapter 5.2.1, gives an efficiency of $\eta_b = 0.891\frac{0.929}{0.873} = 0.948$. The real battery pack's efficiency is probably somewhere in the middle of those two extremes.

The fuel consumption rate per hour for the two cases are 119 kg/hour in simulation one and 131.1 kg/hour in simulation two, which means that the battery assisted genset uses 9.23% less fuel. The fuel consumption was found by looking at the BSFC of the engine and power produced

by the connected generator in each time step. Using the BSFC means that the generator losses are not included, but the genset losses are found to be less than one percent. Thus the figures are fairly accurate. The generator should be of the same magnitude for both simulations, so it has not affected the percentage result. The load and BSFC plots are proportionally inverse of each other, which makes sense based on the BSFC plot in figure 3.2.

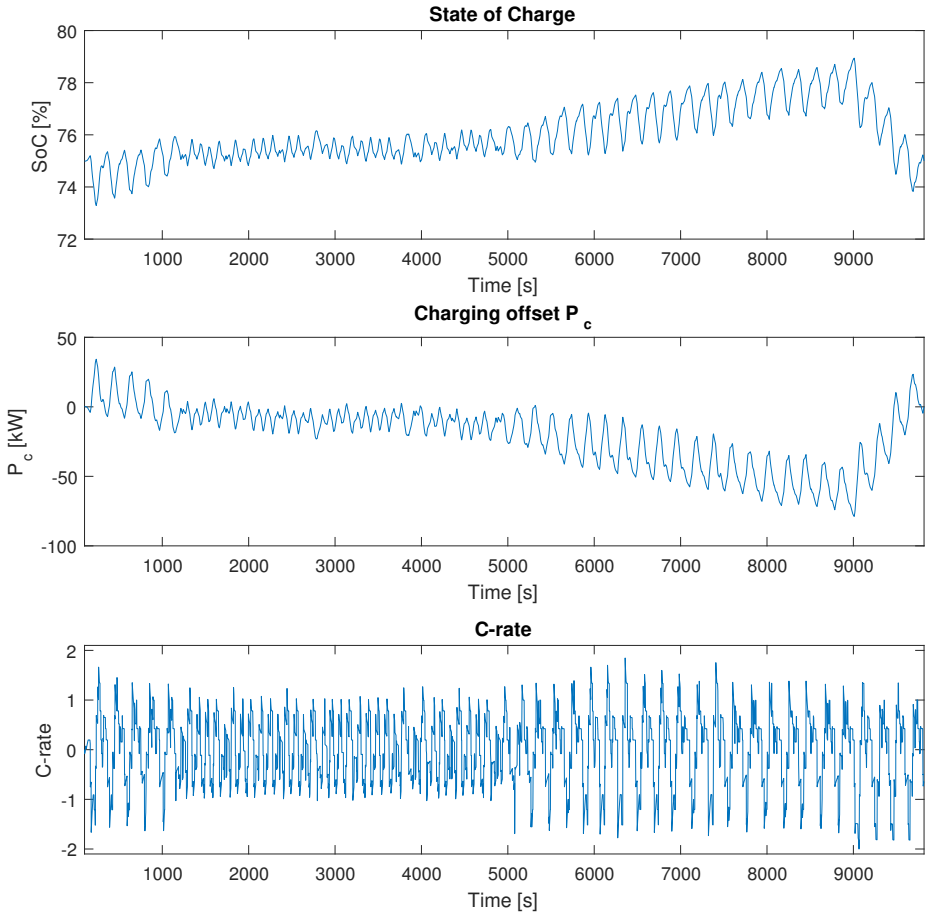

Figure 5.11: Battery pack SoC, charging offset and C-rate

Looking at the SoC plot in figure 5.11, the SoC never drifts off further from the set optimal level of 75% to alter the dynamic limits. The sudden shift down from t=9000 s and till the end of the simulation, is due to the shift in the genset's upper limit, down to 600 kW, as mentioned in the case setup. The SoC is trending upwards at t= 9000s, so it might look like it is going to pass 80%, but a simulation run for 40 000 s confirms that the SoC settles between 76% and 79.5%. Thus the charging offset is sufficient to keep the SoC from diverging from the set limits in this case.

The C-rate plot in figure 5.11 shows that the battery pack operates well within the set limits of C-rate = ± 2.

5.2.3 Discussion

The battery pack's SoH depends on many factors, like calendar ageing, DoD, temperature, C-rates etc. The temperature arises from the heat dissipated by the inner resistance of the battery.

According to the battery pack manufacturer Corvus, there is no problem to achieve a satisfactory cooling solution if the C-rate is kept within ±2 most of the time. How much the battery pack's SoH is reduced by large C-rates is a function of the length of the burst. According to Corvus, there is no problem letting the battery pack handle, e.g. a C-rate of up to ±6 for short bursts of up to 10 s. If the C-rate is allowed to exceed the limits of ±2 set in this thesis, there must be a control system in place that ensures that the duration of the burst is limited. It is hard to anticipate the battery pack's lifetime in a case study like this, but with bounded C-rates, proper cooling and a shallow DoD of less than 10%, the lifetime is expected to be satisfactory. The information from Corvus was received in a phone call to their sales desk.

The amount of energy that is burnt off, as discussed in section 3.5 when the load level is below the gensets combined lower limit, is not mentioned in the results, since the energy amount is neglectable. The instantaneous power can be large, but it occurs rarely, and in short bursts, so the total amount of energy is very small. In reality, the cranes used on Grieg Star's ships have a local power limiting system, which ensures that they never overload the ship's power system. All hoisting and luffing actions have a two-second ramp up time, to avoid sudden changes in power, such that the load profile will be much more gentle than the one used in this simulation. Thus the largest maintenance cost reduction comes from the fact that there is one less genset running while the battery is active.

Ovrum and Bergh (2015) found that a battery pack of size 312 kWh in the same Grieg Star crane scenario had a payback time of less than a year if the battery pack replaces one of the gensets already in the planning phase. They also state that the benefits they had found are conservative, based on that it does not include the effect of that combustion engines are less efficient during load transients. This effect is found to be negligible by a new study by Yum et al. (2017), as long as the engine's load is above 30-40%. The engines are not expected to run at such low loads while a battery pack is active. Thus their results are not believed to be understated with respect to that matter.

This thesis has not focused on specific economical numbers, and the fuel saving estimates are lower than that of Ovrum and Bergh (2015), but the author believes that the results can be found to be of the same magnitude if all parameters are tuned, and the control strategies are optimised. Thus there is a clear economical incentive for ship owners to consider a hybrid power plant.

6 Conclusion and Further Work

This thesis has focused on developing a simulation model that can investigate the effects of including a battery pack inside a marine power plant. The developed model was created with bond graph modelling and implemented in the bond graph software 20-sim. Three control strategies were created to test the model, where each strategy had a different focus. The average control strategy focused on making the gensets' handle the average power, thus minimising the gensets' power rate of change. The power rate of change strategy's objective was to reduce the gensets' power rate of change to a set threshold while minimising the need for battery capacity. The dynamic limit control strategy focused on fuel reduction, by allowing the gensets' to work within their most efficient load interval, and includes the power rate of change strategy while the load is inside the given interval.

The scope of work has been altered from the original, that can be seen at the beginning of this thesis. The original scope of work states that the power system model should be implemented in a crane model, which was created by Fredrik Gyberg in his master's thesis. That plan was found to be to complex, both with regards to modelling and computational power, i.e. simulation speed. Thus the crane model was not included, and the load was applied directly based on test data from Grieg Star. This decision has probably lead to better results since the crane model would have introduced even more modelling uncertainties.

A new control strategy was developed after case study 1, where each of the control strategies was tested. The new control strategy, which then would be used in case study 2, combined the average load and dynamical limit, to gain the benefits of both strategies. The new control strategy has dynamical limits to keep the engines' at an optimal load level and makes the engines' handle the average load while the average is within the given limits.

In case study 2, which was this thesis main case study, the results of two simulations where compared. One simulation ran two gensets, and the other ran one genset assisted by a battery pack. The load profile applied was set to resemble an electric crane operation on a dry bulk carrier. The results show that if one genset is replaced with a 362 kWh battery pack, the fuel consumption rate can be reduced by 9.23%, while the maintenance costs for the operation can be reduced by over 50%. The figures are believed to be conservative, since the battery pack model's efficiency rating is lower than the real battery pack, due to an added resistance to make the model stable. The results show that implementing a battery pack can give significant reductions both environmentally and economically, and should be implemented on all ships that have a diesel-electric power system.

For further work, the model needs to be calibrated by a hybrid lab trial, to figure out how close the simulation results are to the results from a real power system. This model is only meant to be a case study that investigates the general benefits, and will not give accurate results for specific cases. For a specific case, each sub model would have to be reworked to accurately resemble the components used.

References

Aarflot, Ø. A. (2010). Batteriovervåking.

Ådnanes, A. K. (2003). Maritime electrical installations and diesel electric propulsion.

Borutzky, W. (2009). Bond Graph Methodology.

DNV GL AS (2017). RULES FOR CLASSIFICATION: SHIPS Pt4Ch8. Technical report.

Erdinc, O., Vural, B., and Uzunoglu, M. (2009). A dynamic lithium-ion battery model considering the effects of temperature and capacity fading. In 2009 International Conference on Clean Electrical Power, pages 383–386. IEEE.

Garrett, T. K. (2000). Motor Vehicle.

Geertsma, R., Negenborn, R., Visser, K., and Hopman, J. (2017). Design and control of hybrid power and propulsion systems for smart ships: A review of developments. Applied Energy, 194:30–54.

He, H., Xiong, R., Guo, H., and Li, S. (2012). Comparison study on the battery models used for the energy management of batteries in electric vehicles. Energy Conversion and Management, 64:113–121.

Hu, X., Li, S., and Peng, H. (2012). A comparative study of equivalent circuit models for Li-ion batteries. Journal of Power Sources, 198:359–367.

Iizuka, N., Pitt, A., Buckland, R., Lee, E. G., Rahbari, E., Buiter, W., Lee, W., Sasaki, T., D 'antonio, P., Levkovich, T., Saunders, M., Lorenzen, H., Savvantidou, S., Edwards, R., Lubin, D., Schofield, M., Elliot, R., Menuet, G., Shen, M., Morse, E. L., Shoup, J., Goldin, I., Morse, R., Spittler, M. D., Hale, J., Murashima, K., Yuen, A., Horowitz, K., and Peterson, D. M. (2015). Citi GPS: Global Perspectives and Solutions - Investment Themes in 2015.

International Energy Agency (IEA) (2017). WORLD ENERGY BALANCES: AN OVERVIEW Global trends.

International Maritime Organization (IMO) (2011). MARPOL : consolidated edition 2011 : articles, protocols, annexes and unified interpretations of the international convention for the prevention of pollution from ships, 1973, as modified by the 1978 and 1997 protocols.

International Maritime Organization (IMO) (2014). Third IMO greenhouse gas study 2014. Technical report, London.

Kongsberg Maritime (2017). https://www.km.kongsberg.com/ks/web/nokbg0240.nsf/AllWeb/A297BDC3A79BBB36C125726B00387597?OpenDocument Accessed: 2017-08-23.

Kothari, D. P. and Nagrath, I. J. (2010). Electric machines. Mc Graw Hill India.

Lindtjørn, J. and Kanerva, S. (2016). Onboard DC Grid Signals Power Change. Sea Technology, 57(7):10–13.

Martínez-Rosas, E., Vasquez-Medrano, R., and Flores-Tlacuahuac, A. (2011). Modeling and simulation of lithium-ion batteries. Computers and Chemical Engineering, 35(9):1937–1948.

Ménard, L., Fontès, G., and Astier, S. (2010). Dynamic energy model of a lithium-ion battery. Mathematics and Computers in Simulation, 81(2):327–339.

Ovrum, E. and Bergh, T. F. (2015). Modelling lithium-ion battery hybrid ship crane operation. Applied Energy, 152:162–172.

Pedersen, E. and Engja, H. (2014). Mathematical Modelling and Simulation of Physical Systems.

Sahm, D. (1979). A two-axis, bond graph model of the dynamics of synchronous electrical machines. Journal of the Franklin Institute, 308(3):205–218.

Scrosati, B. and Garche, J. (2010). Lithium batteries: Status, prospects and future. Journal of Power Sources, 195(9):2419–2430.

Skjong, S. and Pedersen, E. (2017). A Real-Time Simulator Framework for Marine Power Plants with Weak Power Grids. Elsevier - Mechatronics, Under review.

Tarascon, J.-M. (2015). Electrochemical Energy Storage.

United Nations Conference on Trade and Development (2017). REVIEW OF MARITIME TRANSPORT 2016. UNITED NATIONS.

Weicker, P. (2013). A Systems Approach to Lithium-Ion Battery Management.

Wood, A. J. (2014). Power generation, operation and control.

Yum, K. K., Lefebvre, N., and Pedersen, E. (2017). An experimental investigation of the effects of cyclic transient loads on a turbocharged diesel engine. Applied Energy, 185:472–481.

Zecca, A. and Chiari, L. (2010). Fossil-fuel constraints on global warming. Energy Policy, 38(1):1–3.

Zu, C.-X., Li, H., Denturck, K., Langenhove, H. V., Ghyoot, W., Tytgat, J., Vandeputte, K., Moshkovich, M., and Levi, E. (2011). Thermodynamic analysis on energy densities of batteries. Energy & Environmental Science, 4(8):2614.

Appendix A. Attachments

The following attachments can be found inside Attachments.zip

Marine power plant with battery model - final.emx: The bond graph model

random_2_cranes_200_pass_1.csv: Load profile used in case 2

generate_loadcycle.py: The python code used to generate the load data set

Appendix B. Model parameters

$P_{\max}$	960 kW
r	10 kgm^2/s
J_e	500 kgm^2
J_G	500 kgm^2

Table B.1: Engine parameters

L_d	0.0007728204790303 Ω
L_q	0.00052572821702741377 Ω
L_f	0.606375 Ω
L_D	0.59873297979798 Ω
L_Q	0.39874544450183647000 Ω
L_{df}	0.016217597392891 Ω
L_{dD}	0.016217597392891 Ω
L_{fD}	0.576975 Ω
L_{qQ}	0.01044314983633161900 Ω
R_d	0.00497 Ω
R_q	0.00497 Ω
R_f	0.315 Ω
R_D	6.2165656565657 Ω
R_Q	9.7575355831038 Ω
n_p	5
T	0.001 s

Table B.2: Generator parameters

V_{ref}	690 V
K_p	5
T_i	5 s
Saturation	$\pm 100V$

Table B.3: AVR parameters

-

K_p	1e-5 V/VAr
T_i	1 s

Table B.4: Reactive sharing parameters

ω_{ref}	24 π rad/s
K_p	0.1 kgs/rad
T_i	0.1 s
T_d	50 s
N_d	10
Saturation	[0, 0.26] kg

Table B.5: Active sharing/Governor parameters

n_s	250
n_p	See each simulation
R_0	$0.8m\Omega$
R_{th}	$0.2m\Omega$
R_{wire}	$\text{sat}(0.11 - R_0, pack, 0, 1)\Omega$
τ_B	15 s
η_{acdc}	0.99
PF_{acdc}	0.96
η_{dcdc}	0.99

Table B.6: Battery pack parameters

$P_{\text{g,max}}$	900 kW
$P_{\text{g,min}}$	100 kW
T_f	0.001 s
$C_{\text{in,max}}$	2
$C_{\text{out,max}}$	2

Table B.7: Global control parameters

T_{avg}	300 s
SOC_{sp}	75 %
K_c	30000 kW/%
T_f	1 s
P_{dl}	10 kW
P_{lsl}	250 kW

Table B.8: Average load control parameters

$\dot{P}_{\text{g,max}}$	50 kW/s
SOC_{sp}	75 %
K_c	30000 kW/%
T_f	0.01 s

Table B.9: Power rate limit control parameters

-

$K_{p,L}$	25 kW/%
$K_{p,U}$	25 kW/%
T_f	0.01 s
SOC_L	See each simulation
SOC_U	See each simulation
$P_{g,L}$	See each simulation
$P_{g,U}$	See each simulation

Table B.10: Dynamical limit control parameters

Appendix C. Generate Load Profile: Python code

The function takes two parameters, where the first is the number of active cranes, and the other is the number of times the load cycle should run. The resulting load profile is output in a csv-file, which is stored in the same folder the script is executed in.

```
import random
import sys
import os.path

def generate_loaddata(cranes,passes):
 hotel = 375
 loadprofile = {}

 for i in range(0,100):
  loadprofile[i] = hotel

 for i in range(100,400*passes):
  loadprofile[i] = hotel

 for j in range(0,cranes):
  usedtime = 100 + random.randint(0,30)
  for i in range(0,passes):
   #Load cycle no 1
   step1 = random.randint(45,85)

   for i in range(usedtime,usedtime+step1):
    loadprofile[i] = loadprofile[i] + 20

   usedtime += step1
   step2 = 45

   for i in range(usedtime,usedtime+step2):
    loadprofile[i] = loadprofile[i] + 372

   usedtime += step2
   step3 = 14

   for i in range(usedtime,usedtime+step3):
    loadprofile[i] = loadprofile[i] + 475
```

```
    usedtime += step3
    step4 = 27

    for i in range(usedtime,usedtime+step4):
     loadprofile[i] = loadprofile[i] + 80

    usedtime += step4
    step5 = 27

    for i in range(usedtime,usedtime+step5):
     loadprofile[i] = loadprofile[i] - 212

    usedtime += step5
    step6 = random.randint(10,20)

    for i in range(usedtime,usedtime+step6):
     loadprofile[i] = loadprofile[i] + 20

    usedtime += step6
    step7 = 15

    for i in range(usedtime,usedtime+step7):
     loadprofile[i] = loadprofile[i] + 125

    usedtime += step7
    step8 = 30

    for i in range(usedtime,usedtime+step8):
     loadprofile[i] = loadprofile[i] - 89

  i=1
  while True:
   filename = "random_" + str(cranes) + "_cranes_" +
   str(passes) + "_pass_" + str(i) + ".csv"
   if os.path.isfile(filename):
    i += 1
   else:
    break
  file = open(filename, 'w')
  file.write('t,load\n')
  for i in range(0,len(loadprofile.keys())):
   file.write(str(i) + "," + str(loadprofile[i])+"\n")

generate_loaddata(int(sys.argv[1]), int(sys.argv[2]))
```